- 1 Plant-Necrotroph Co-transcriptome Networks Illuminate a Metabolic Battlefield
- 2 Wei Zhang^{1,2}, Jason A. Corwin³, Daniel Copeland², Julie Feusier², Robert Eshbaugh²,
- 3 David E. Cook¹, Susana Atwell², and Daniel J. Kliebenstein^{2,4*}
- ⁴ ¹Department of Plant Pathology, Kansas State University, 1712 Clafflin Road, Throckmorton
- 5 Hall, Manhattan, KS, 66506, USA
- ⁶ ²Department of Plant Sciences, University of California, Davis, One Shields Avenue, Davis, CA,
- 7 95616, USA
- ³Department of Ecology and Evolution Biology, University of Colorado, 1900 Pleasant Street,
- 9 334 UCB, Boulder, CO, 80309-0334, USA
- ⁴DynaMo Center of Excellence, University of Copenhagen, Thorvaldsensvej 40, DK-1871,
- 11 Frederiksberg C, Denmark
- 12 *Correspondence: Daniel J. Kliebenstein, Department of Plant Sciences, University of
- 13 California, Davis, One Shields Ave, Davis, CA, 95616, USA.
- 14 <u>kliebenstein@ucdavis.edu</u>
- 15 Phone: 530-754-7775
- 16 Running title: Co-transcriptome Networks between Arabidopsis and Botrytis cinerea
- 17 Keywords: Host-pathogen Interaction, Co-transcriptome, Gene Co-expression Network,
- 18 Pathosystem, Arabidopsis, Botrytis cinerea
- 19
- 20
- 21

22 Abstract

23 A central goal of studying host-pathogen interaction is to understand how host and pathogen 24 manipulate each other to promote their own fitness in a pathosystem. Co-transcriptomic 25 approaches can simultaneously analyze dual transcriptomes during infection and provide a 26 systematic map of the cross-kingdom communication between two species. Here we used the 27 Arabidopsis-B. cinerea pathosystem to test how plant host and fungal pathogen interact at the 28 transcriptomic level. We assessed the impact of genetic diversity in pathogen and host by 29 utilization of a collection of 96 isolates infection on Arabidopsis wild-type and two mutants with 30 jasmonate or salicylic acid compromised immunities. We identified ten B. cinerea gene co-31 expression networks (GCNs) that encode known or novel virulence mechanisms. Construction of 32 a dual interaction network by combining four host- and ten pathogen-GCNs revealed potential 33 connections between the fungal and plant GCNs. These co-transcriptome data shed lights on the 34 potential mechanisms underlying host-pathogen interaction. 35

- 36
- 37
- 38
- 39
- 40

41 INTRODUCTION

42 How a host and pathogen manipulate each other within a pathosystem to facilitate their own 43 fitness remains a long-standing question. The difference between the pathogen's ability to infect 44 and the host's ability to resist generates the resulting disease symptomology. This interaction 45 forces host-pathogen dynamics to shape the genomes of the two species via adaptive responses to 46 each other (Dangl and Jones, 2001; Bergelson et al., 2001; Benton, 2009; Kanzaki et al., 2012; 47 Karasov et al., 2014). Plants have evolved a sophisticated set of constitutive and inducible 48 immune responses to cope with constant selective pressures from antagonistic microbes (Jones 49 and Dangl, 2006). Reciprocally, plant pathogens have also evolved a variety of different invasion 50 and virulence strategies to disarm or circumvent plant defense strategies (Glazebrook, 2005; 51 Toruno et al., 2016). This has resulted in complex relations between plant hosts and fungal 52 pathogens for survival and fitness.

53 The plant innate immune system includes several functional layers with overlapping functions to 54 detect and defend against phytopathogens. This multi-layer immune system can be categorized 55 as a signal monitor system to detect invasion, local and systemic signal transduction components 56 to elicit and coordinate responses, and defensive response proteins and metabolites focused on 57 combatting the invading pathogen (Tsuda and Katagiri, 2010; Corwin and Kliebenstein, 2017). 58 These functional layers, as well as the components within them, are highly interconnected and 59 tightly regulated by the host plant to respond appropriately to various phytopathogens (Couto 60 and Zipfel, 2016; Tang et al., 2017). For instance, Arabidopsis utilizes a complex signaling 61 network to regulate the production of indole-derived secondary metabolites, such as camalexin 62 and indole glucosinolates, that contribute to resistance against pathogens (Kliebenstein et al., 63 2005; Clay et al., 2009; Bednarek et al., 2009; Frerigmann et al., 2016; Xu, J. et al., 2016;

64 Mine et al., 2018). This layered immune system provides pathogens with numerous targets in the 65 plant immune system that the pathogen can utilize, evade or attack. Most biotrophic pathogens, 66 evolved from commensal microbes, attempt to dismantle the plant immune system by injecting 67 effector proteins into host cells or the inter-cellular space (Dangl and Jones, 2001; Buttner and 68 He, 2009; Stergiopoulos and de Wit, 2009). For example, the biotrophic bacterial pathogen 69 *Pseudomonas syringae* can utilize the jasmonic acid (JA) signaling pathway through the 70 production of a JA-mimic, coronatine, to enhance its fitness (Mittal and Davis, 1995; Brooks et 71 al., 2005; Cui et al., 2018). Alternatively, necrotrophic pathogens, which often evolved from 72 environmental saprophytic microbes, can utilize toxic secondary metabolites, small secreted 73 proteins, and small RNAs to aggressively attack host defenses while also defending against host-74 derived toxins (Choquer et al., 2007; Arbelet et al., 2010; Mengiste, 2012; Weiberg et al., 75 2013; Kubicek et al., 2014; Macheleidt et al., 2016). In addition, pathogens can directly resist 76 downstream defenses as is done by *B. cinerea*, where it has an ATP-binding cassette (ABC) 77 transporter BcatrB that provides resistance by exporting camalexin from the pathogen cell 78 (Stefanato et al., 2009). This high level of interactivity between the immune system and 79 pathogen virulence mechanisms generates the final level of disease severity. However, a 80 functional description of this combative cross-kingdom communication between a plant host and 81 necrotrophic pathogen remains elusive.

Co-transcriptomic approaches whereby the host and pathogen transcriptomes are simultaneously
analyzed provide the ability to systematically map the cross-kingdom communication between
plant hosts and their pathogens, both for individual genes and gene co-expression network
(GCN) levels (Stuart et al., 2003; Musungu et al., 2016; Zhang, W. et al., 2017; Lanver et al.,
2018; McClure et al., 2018). Recent advances have enabled the measurement of pathogen *in*

87	planta transcriptome. For example, in planta measurements of the pathogens' transcriptome
88	within the biotrophic Arabidopsis-Pseudomonas syringae pathosystem has enabled the
89	investigation of early effects on Arabidopsis host immunity and the consequent effects on
90	bacterial growth (Nobori et al., 2018). This enabled the identification of a bacterial iron
91	acquisition pathway that is suppressed by multiple plant immune pathways (Nobori et al., 2018).
92	This shows the potential for new hypothesis to be generated by a co-transcriptome approach
93	(Swierzy et al., 2017; Westermann et al., 2017; Lee et al., 2018).
94	The Arabidopsis-B. cinerea pathosystem is well suited for exploring plant-pathogen interaction
95	to understand host defenses and necrotrophic virulence in ecological and agricultural settings. B.
96	cinerea is a necrotrophic generalist pathogen that attacks a broad range of diverse plant hosts,
97	including dicots, gymnosperms, and even bryophytes (Williamson et al., 2007). This
98	necrotrophic pathogen is endemic throughout the world and can cause severe pre- and post-
99	harvest losses in many crops. A high level of standing natural genetic variation within B. cinerea
100	population is hypothesized to facilitate the extreme host range of <i>B. cinerea</i> . This genetic
101	variation affects nearly all known B. cinerea virulence strategies, including penetration and
102	establishment, evading detection, and combatting/coping with plant immune responses (Atwell
103	et al., 2015; Walker et al., 2015; Corwin, Subedy et al., 2016). For example, a key virulence
104	mechanism is the secretion of phytotoxic secondary metabolites, including the sesquiterpene
105	botrydial (BOT) and the polyketide botcinic acid (BOA) that trigger plant chlorosis and host cell
106	collapse (Deighton et al., 2001; Colmenares et al., 2002; Wang et al., 2009; Rossi et al., 2011;
107	Ascari et al., 2013; Porquier, A. et al., 2016). These metabolites are linked to virulence, but
108	some pathogenic field isolates fail to produce either compounds pointing to additional
109	pathogenic strategies. The combination of a high level of genetic diversity and extensive

110 recombination means that a population of *B. cinerea* is a mixed collection of virulence strategies111 that can be used to interrogate by the co-transcriptome.

112 In the present study, the Arabidopsis-B. cinerea pathosystem is used to test how the 113 transcriptomes of the two species interact during infection and assess how natural genetic 114 variation in the pathogen impacts disease development. Isolates were inoculated on Arabidopsis 115 Col-0 wild-type (WT) in conjunction with immune-deficient hormone mutants *coil-1* (jasmonate 116 defense signaling) and *npr1-1* (salicylic acid defense signaling). A collection of 96 isolates of *B*. 117 *cinerea* was used for infection, which harbor a wide scope of natural genetic variation within the 118 species (Atwell et al., 2015; Corwin et al., 2016; Zhang et al., 2016; Corwin, Copeland et al., 119 2016; Zhang et al., 2017; Soltis et al., 2018; Fordyce et al., 2018). From individual infected 120 leaves, both Arabidopsis and *B. cinerea* transcripts at 16 hours post-infection (HPI) were 121 simultaneously measured. Arabidopsis transcripts was analyzed previously to identify four host-122 derived GCNs that are sensitive to natural genetic variation in *B. cinerea* (Zhang et al., 2017). In 123 present analysis, ten fungal pathogen-derived GCNs were identified, which encode either known 124 or novel virulence mechanisms within the species. Some of these B. cinerea GCNs responsible 125 for BOT production, exocytosis regulation and copper transport are highly linked with the host's 126 defense phytohormone pathways. By combining the plant host- and pathogen-GCNs into a single 127 network, a dual-transcriptomic network was constructed to identify potential interactions 128 between the components of plant host innate immune system and fungal pathogen virulence. 129 These connections highlight potential targets for fungal pathogen phytotoxins and prevailing 130 counter-responses from plant host. Collectively, co-transcriptomic analysis shed lights on the 131 potential mechanisms underlying how the host and pathogen combat each other during infection

and illustrate the continued need for advancements of *in planta* analysis of dual-speciesinteraction.

134 **RESULTS**

135 Genetic Variation in Pathogen and Hosts Influence B. cinerea Transcriptome

136 To investigate how genetic variation within a pathogen differentially interacts with plant host 137 immunity at the transcriptomic level, we profiled the *in planta* transcriptomes of 96 B. cinerea 138 isolates infection across three host genotypes, the Arabidopsis accession Col-0 WT and two 139 immune-signaling mutants *coil-1* and *npr1-1* that are respectively compromised in JA or 140 salicylic acid (SA) driven immunity. This previously described collection of 96 isolates 141 represents a broad geographical distribution and contains considerable natural genetic variation 142 that affects a diversity of virulence strategies within *B. cinerea* (Denby et al., 2004; Rowe and 143 Kliebenstein, 2007; Atwell et al., 2015; Corwin et al., 2016; Zhang et al., 2016). Four 144 independent biological replicates across two separate experiments per isolate/genotype pair were 145 harvested at 16HPI for transcriptome analysis. A total of 1,152 independent RNA samples were 146 generated for library preparation and sequenced on Illumina HiSeq platform (NCBI accession 147 number SRP149815). These libraries were previously used to study Arabidopsis transcriptional 148 responses to natural genetic variation in *B. cinerea* (Zhang et al., 2017). Mapping the dual-149 transcriptome reads against the *B. cinerea* reference genome (B05.10), we identified 9,284 150 predicted gene models with a minimum of either 30 gene counts in one isolate or 300 gene 151 counts across 96 isolates. The total of identified genes corresponds to ~79% of the 11,701 152 predicted encoding genes in B05.10 reference genome (Van Kan et al., 2017). The two different

thresholds allowed the identification of pathogen transcripts that express only in a specificisolate.

155 Measuring the abundance of individual pathogen transcripts in relation to the host transcripts can 156 be used as a molecular method to estimate fungal biomass (Blanco-Ulate et al., 2014). Given 157 this, we hypothesized that the fraction of total reads that map to B. cinerea might be a 158 biologically relevant indicator of pathogen virulence (Figure 1-source data 1). Comparing B. 159 cinerea transcript abundance at 16HPI to lesion development at 72HPI revealed a significant partial correlation in the WT Col-0 ($R^2 = 0.1101$, *P*-value = 0.0016, Figure 1). In contrast to WT, 160 161 the early transcriptomic activities of most *B. cinerea* isolates were more vigorous in the two 162 Arabidopsis mutants, resulting in a significant curvilinear relationship between total fraction of 163 B. cinerea reads and final lesion area (P-value = 3.914e-07, P-value = 0.0001, respectively, 164 Figure 1). Interestingly, the total reads fraction was better correlated with final lesion area in *coil-1* ($R^2 = 0.2562$) than either WT ($R^2 = 0.1101$) or *npr1-1* ($R^2 = 0.161$). This suggests that 165 166 early transcriptomic activity from the pathogen can be a partial indicator of pathogen virulence, 167 but also depends on the respective resistance from the plant host.

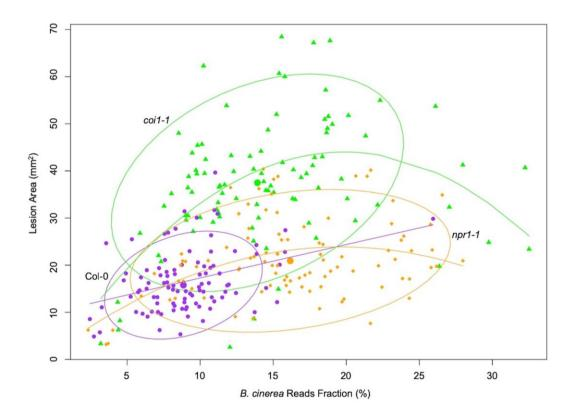


Figure 1. Correlation between earlier estimated *B. cinerea* biomass and later lesion area. Model-corrected lesion area means were estimated using the linear model on the six replicates data from three Arabidopsis genotypes at 72-hours post-infection with 96 *B. cinerea* isolates. Estimated biomass of *B. cinerea* was calculated using the linear model-corrected fraction of *B. cinerea* mapped reads against total mapped reads to Arabidopsis and *B. cinerea* reference genomes. RNA-Seq analysis was conducted at 16-hours post-infection for each pathosystem. Three Arabidopsis genotypes are wild-type Col-0 (purple dot), jasmonate insensitive mutant *coi1-1* (green triangle), and salicylic acid insensitive mutant *npr1-1* (orange diamond). The 90% confidence ellipse intervals are plotted for each Arabidopsis genotype for references. Quadratic regression lines are: Col-0: y = -0.00059x² + 0.729x + 10.037, *P* = 0.0016, adjusted R² = 0.1101; *coi1-1*: y = -0.117x² + 4.44x - 0.1585, *P* = 3.914e-07, adjusted R² = 0.2562; *npr1-1*: y = -0.0579x² + 2.26x + 1.673, *P* = 0.0001, adjusted R² = 0.161.

168

169 Plant defense phytohormone networks, like SA and JA, help shape the immune responses of a 170 plant host while also shape the virulence gene expression within bacterial pathogens, such as 171 Pseudomonas syringae (Nobori et al., 2018). To test how variation in host SA/JA-signaling 172 influences the fungal pathogen transcriptome, we applied a generalized linear model linked with 173 negative-binomial function (nbGLM) to each B. cinerea transcript across the experiment. This analysis allowed us to estimate the relative broad-sense heritability (H^2) of genetic variation from 174 175 the pathogen, plant host, or their interaction contributing to each transcript (Figure 2-source data 176 1-3). Of the 9,284 detectable B. cinerea transcripts, 8,603 and 5,244 transcripts were

177 significantly influenced by genetic variation in pathogen and host, respectively (74% and 45% of 178 predicted *B. cinerea* gene models, respectively) (Figure 2A, Figure 2-source data 3 and 4). While 179 this result shows that the plant phytohormone pathways influence B. cinerea gene expression, the 180 variation in host defense responses (average $H^2_{Host} = 0.010$) has far less influence on *B. cinerea* 181 gene expression than that of the pathogens' own natural genetic variation (average $H^2_{\text{Isolate}} =$ 182 0.152). The host defense hormones also affected *B. cinerea* gene expression in a genotype-by-183 genotype dependent manner on 4,541 genes (39% of B. cinerea predicted gene models, average 184 $H^{2}_{\text{Isolate x Host}} = 0.116$) (Figure 2B-2I). Illustrating this potential for host x pathogen interactions 185 on pathogen gene expression are the two genes encoding the well-studied polygalacturonase 1 186 (*Bcpg1*) and oxaloacetate acetyl hydrolase. The two virulence associated genes showed dramatic 187 expression variation across 96 isolates in different host backgrounds (Figure 3, Figure 3-figure 188 supplemental 1, and Figure 2-source data 1). Extending this to 500 genes showing the strongest 189 host x pathogen effect showed that there is a wide range of patterns that differs in the host *coil-1* 190 or *npr1-1* background with diverse pathogen strain specific patterns (Figure 4). One potential 191 complication of this analysis is for sequence variation between the reference B05.10 genome and 192 the diverse strains to create artificially low expression estimates. However, very few genes 193 showed consistently low expression within a strain and instead when a gene showed no 194 expression in one host genotype, it was expressed in a different host genotype (Figure 3 and 195 Supplementary File 1). This conditionality argues against a sequencing error as the sequence has 196 not altered. The genes that did show a loss of expression across all host genotypes within a strain 197 (i.e. BOT and BOA genes) were frequently linked to whole gene deletions that abolished their 198 expression (Soltis et al., 2019). Thus, while there are likely some sequence variation associated 199 expression errors, they are not a dominant signature in the data. Thus, within the Arabidopsis/B.

cinerea pathosystem the

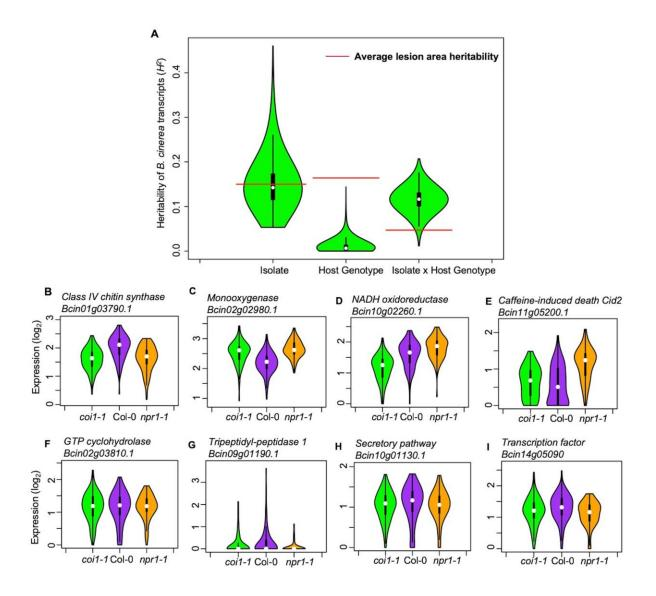


Figure 2. Transcriptomic responses of *B. cinerea* **on Arabidopsis are controlled by genetic variation in pathogen population, host genotypes, and their interaction.** (A) Distribution of broad-sense heritability (*H*²) of *B. cinerea* transcripts contributed by genetic variation in the *B. cinerea*, Arabidopsis genotypes, and the interaction between pathogen and host. Violin plots illustrating the distribution of *H*² for transcripts from 96 *B. cinerea* isolates infecting on Arabidopsis genotypes. Heritability is partitioned across the different sources, 96 pathogen genotypes = "Isolate", plant genotypes Col-0, *coi1-1* and *npr1-1* plant genotypes = "Host", and the corresponding interaction. The transcriptomic analysis was conducted by sequencing mRNA extracted from *B. cinerea* infected Arabidopsis leaves at 16-hours post-infection. Red lines indicate the average broad-sense heritability values of lesion area caused by isolates, Arabidopsis genotypes, and their interaction. (B) to (E) Expression profiles of *B. cinerea* transcripts significantly influenced by host genotypes. The model-corrected means (log₂) for *B. cinerea* transcript were used for plotting. The Arabidopsis genotypes, wild-type Col-0 (purple), jasmonate insensitive mutant *coi1-1* (green), and salicylic acid mutant *npr1-1* (orange), are shown on the x axis. *B. cinerea* transcripts are: (B) *Bcin01g03790.1*, class IV chitin synthase; (C) *Bcin02g02980.1*, Monooxygenase; (D) *Bcin10g02260.1*, NADH oxidoreductase; (E) *Bcin11g05200.1*, caffeineinduced death Cid2; (F) to (I) Expression profiles of *B. cinerea* transcripts significantly influenced by the interaction between pathogen and host genotypes. (F) *Bcin02g03810.1*, GTP cyclohydrolase; (G) *Bcin09g01190.1*, Tripeptidyl-peptidase 1; (H) *Bcin10g01130.1*, in secretory pathway; (I) *Bcin14g05090.1*, a transcription factor.

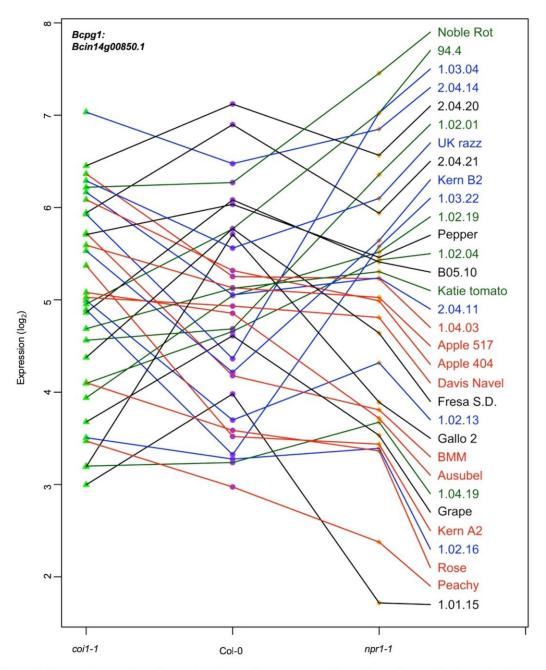


Figure 3. Expression profiles of an endopolygalacturonase gene *Bcpg1* from diverse *B. cinerea* isolates across **Arabidopsis genotypes.** Rank plot shows the relationship of *Bcpg1* expression from 32 diverse *B. cinerea* isolates (right) across three Arabidopsis genotypes (x axis). Three Arabidopsis genotypes are wild-type Col-0 (purple dot), jasmonate insensitive mutant *coi1-1* (green triangle), and salicylic acid mutant *npr1-1* (orange diamond). The model-corrected means (log₂) for the transcript of *Bcpg1* (*Bcin14g00850.1*) encoding an endopolygalacturonase gene are utilized for plotting. The transcript expression levels from the same isolate across three Arabidopsis genotypes are connected with a colored line. The names of 32 isolates are represented with the same colored lines as induced *Bcpg1* expression levels. Black lines indicate the expression levels of *Bcpg1* are higher in *coi1-1* and *npr1-1* than in Col-0. Red lines indicate the higher expression levels of *Bcpg1* are in Col-0. Dark green lines indicate the higher expression levels of *Bcpg1* are in *coi1-1*.

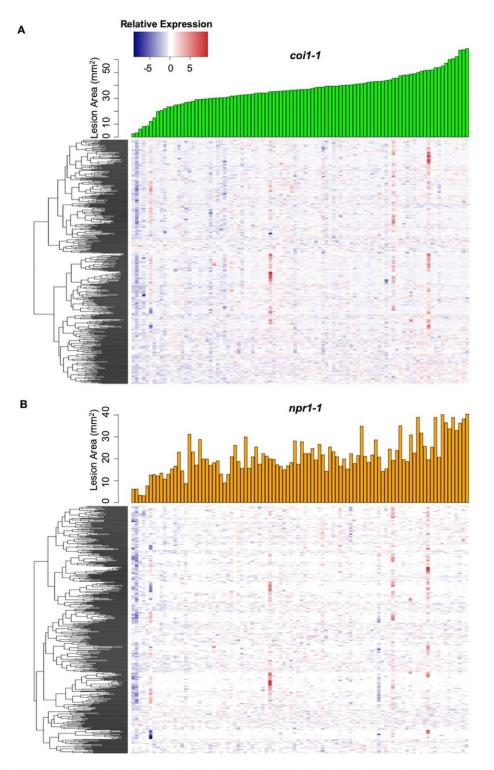


Figure 4. Interaction effects of host genotypes and pathogen isolates on *B. cinerea* transcriptome. Hierarchical clustering of relative expression of 500 genes from 96 *B. cinerea* isolates infection on Arabidopsis mutants *coi1-1* (A) or *npr1-1* (B) are plotted based on pairwise comparison of pathogen gene expression under Col-0. The 500 *B. cinerea* genes with highest broad-sense heritability (H^2) of host X pathogen were used for analysis. Lesion area induced by 96 isolates are compared under *coi1-1* (green bar plot) and *npr1-1* (orange bar plot).

pathogens transcriptional responses are influenced by a blend of the pathogens' natural variation
and its interaction with the host, while there is less evidence for the host's defense responses to
unilaterally affect *B. cinerea*. Future work will hopefully assess how this extends to other hostpathogen systems.

208 Identification of Virulence Factors Among the Early B. cinerea Transcripts

209 This data set also allows us to test for specific *B. cinerea* transcripts whose early expression is 210 associated with later lesion development. These genes can serve as potential biomarkers of 211 overall pathogen virulence and may elucidate the functional mechanisms driving early virulence 212 in the interaction. To find individual pathogen transcripts link with lesion development, we 213 conducted a genome-wide false discovery rate-corrected Spearman's rank correlation analysis 214 between 72HPI lesion area and individual *B. cinerea* transcripts accumulation at 16HPI. We 215 identified 2,521 genes (22% of *B. cinerea* predicted gene models) with significant positive 216 correlations and 114 genes (1% of *B. cinerea* predicted gene models) with significant negative 217 correlations to lesion area across three Arabidopsis genotypes, respectively (P-value < 0.01, 218 Figure 3-source data 1). The top 20 positively correlated *B. cinerea* genes contained all seven 219 genes involved in BOT biosynthesis (Deighton et al., 2001; Colmenares et al., 2002; Wang et 220 al., 2009; Rossi et al., 2011; Ascari et al., 2013; Porquier et al., 2016). In addition to 221 phytotoxins, more than 30 genes of the top 100 lesion-correlated genes encode plant cell wall 222 degrading enzymes, i.e., glucosyl hydrolases, carbohydrate esterases, cellobiose dehydrogenases 223 and *Bcpg1* (Figure 3 and Figure 3-source data 1) (Gerbi et al., 1996; Zamocky et al., 2006; 224 Cantarel et al., 2009; Van Vu et al., 2012; Igarashi et al., 2014; Ingo Morgenstern et al., 2014; 225 Blanco-Ulate et al., 2014; Tien-chye Tan et al., 2015; Courtade et al., 2016; Nelson et al., 226 2017; Pérez-Izquierdo et al., 2017). Additionally, 10 of the top 100 lesion-correlated genes were

227 annotated as putative peptidase activities, which are critical for fungal virulence (Movahedi et

al., 1991; Poussereau, Creton et al., 2001; Poussereau, Gente et al., 2001; ten Have et al.,

229 2004; ten Have et al., 2010). A final classical virulence gene in the top 100 gene list is *Bcoah*

230 (*Bcin12g01020*) encoding oxaloacetate acetyl hydrolase, which is a key enzyme in oxalic acid

biosynthesis that positively contributes to virulence (Figure 3-figure supplemental 1 and Figure

232 3-source data 1) (Greenberg et al., 1994; Williamson et al., 2007; Walz et al., 2008;

233 Schumacher et al., 2012; Schumacher et al., 2015; Tayal et al., 2017). In addition, this method

identified 37 of the top 100 lesion-correlated genes with no gene ontology (GO) terms, which

235 likely represent unknown virulence mechanisms (Figure 3-source data 1). Thus, this approach

readily creates new hypothesis about known and novel pathogen virulence functions.

237 In Planta Virulence Gene Co-expression Networks (GCNs) in B. cinerea

238 To develop a systemic view of fungal pathogen *in planta* gene expression, we used a co-

239 expression approach to identify *B. cinerea* networks that associated with growth and virulence in

240 *planta*. Using solely *B. cinerea* transcriptome at 16HPI from Arabidopsis Col-0 WT infected

241 leaves, we calculated Spearman's rank correlations of gene counts across all *B. cinerea* isolates,

filtered gene pairs with correlation greater than 0.8. We then used the filtered gene pairs as input

to construct GCNs. We identified ten distinct GCNs containing more than five *B. cinerea* genes

244 (Figure 5, Supplementary File 1, Figure 5-figure supplemental 1 and Figure 5-source data 1).

245 The largest GCN with 242 genes contains members responsible for phospholipid synthesis,

eiosome function, and membrane-associated stress signaling pathways (Figure 5-

247 Vesicle/virulence). The biological function of this GCN suggests its role in fungal membrane-

and vesicle-localized processes, which are normally involved with general hyphae growth,

249 fungal cell wall deposition, and exudation of fungal toxins to the intercellular space

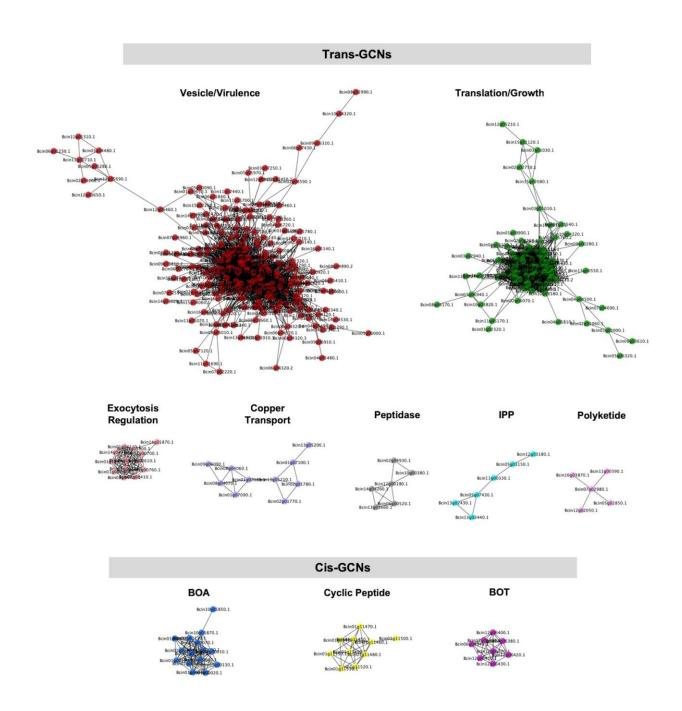


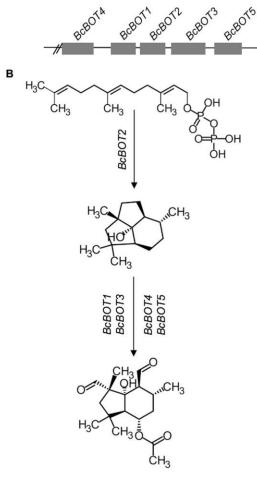
Figure 5. Gene co-expression networks identified from *B. cinerea* transcriptomic responses to Arabidopsis wildtype Col-0 immunity. Ten gene co-expression networks (GCNs) with more than five nodes were identified from 96 *B. cinerea* isolates infecting on Arabidopsis wild-type Col-0. The similarity matrix is computed using Spearman's rank correlation coefficient. Nodes with different colors represent *B. cinerea* genes condensed in GCNs with different biological functions. Edges represent the Spearman's rank correlation coefficients between gene pairs. Trans- and cis-GCNs means GCNs are regulated by trans- and cis-regulatory elements, respectively. GCNs were named after their biological functions, which were determined by hub and bottleneck genes within each network. GCNs are: vesicle/virulence (red), translation/growth (green), exocytosis regulation (pink), cyclic peptide (yellow), peptidase (gray), isopentenyl pyrophosphate (IPP, turquoise), polyketide (violet), botcinic acid (BOA, blue), copper transport (slate blue), botrydial (BOT, purple).

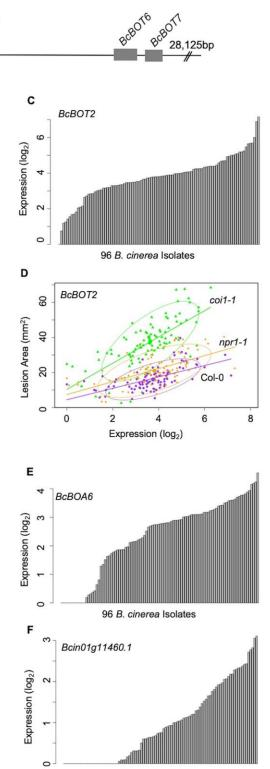
251 (Figure 5-source data 1). The second largest network contains 128 genes that were entirely 252 associated with translation and protein synthesis (Figure 5-TSL/growth and Figure 5-source data 253 1). Of the smaller GCNs identified (5-20 genes), five networks were identified with genes 254 distributed across B. cinerea 16 chromosomes, suggesting that these GCNs arise from 255 coordinated trans-regulation (Figure 5-Trans-networks and Figure 5-figure supplemental 1D, 1F, 256 1H-1J). These networks are associated with diverse array of virulence functions, including the 257 regulation of exocytosis, copper transport, the production of peptidases and isoprenoid 258 precursors (IPP), and polyketide secretion.

259 In contrast to the whole-genome distributed GCNs, three of the smaller GCNs were 260 predominantly comprised of genes tandemly clustered within a single chromosome with no or a 261 few genes on other chromosomes (Figure 5-BOA, -Cyclic Peptide, -BOT, Figure 5-figure 262 supplemental 1C, 1E, and 1G). A functional analysis showed that all of the genes within these 263 networks encoded known or putative biosynthetic enzymes for specialized metabolic pathways. 264 For example, seven genes responsible for BOT biosynthesis cluster on chromosome 12 and form 265 a small GCN with a Zn(II)2Cys6 transcription factor that is specific to the pathway (Figure 6A, 266 6B, Figure 5-figure supplemental 1G and Figure 5-source data 1) (Siewers et al., 2005; Pinedo 267 et al., 2008; Urlacher and Girhard, 2012; Moraga et al., 2016). Similarly, all 13 genes involved 268 in BOA biosynthesis cluster in Chromosome 1 and form a highly connected GCN (Figure 5-269 BOA, Figure 6E, Figure 5-figure supplemental 1C and Figure 5-source data 1) (Dalmais et al., 270 2011; Porquier, Antoine et al., 2019). In addition to previously characterized secondary 271 metabolic pathways, we identified an uncharacterized set of ten genes that cluster on 272 Chromosome 1 (Figure 5-Cyclic Peptide, Figure 6F, Figure 5-figure supplemental 1E and Figure

273 5-source data 1). These genes share considerable homology with enzymes related to







96 B. cinerea Isolates

G

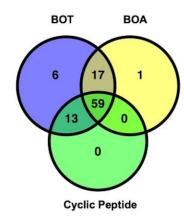


Figure 6. Variation of transcripts accumulation for secondary metabolites production across diverse B. cinerea isolates. Expression profiles of genes responsible for botrydial, botcinic acid, cyclic peptide production across 96 isolates under Arabidopsis wild-type Col-0 are shown. (A) Schematic shows the genomic locus of seven botrydial (BOT) biosynthesis genes clustered together. Exons are represented by gray boxes. Introns and intergenic regions are represented by the grey line. Seven BOT genes are: BcBOT1, BcBOT3 and BcBOT4, encoding a cytochrome P450 monooxygenase, respectively; BcBOT2 encoding a sesquiterpene cyclase; BcBOT5 encoding an acetyl transferase; BcBOT6 encoding a Zn(II)2Cys6 transcription factor, BcBOT7 encoding a dehydrogenase reductase. (B) BOT biosynthesis pathway in B. cinerea. (C) Bar plots compare expression variation of BcBOT2 across 96 B. cinerea isolates in responding to Arabidopsis wild-type Col-0 immunity. The model-corrected means (log₂) of transcripts were used for plotting. (D) Scatter plot illustrates the positive correlations between lesion area and accumulation of BcBOT2 transcript across the 96 isolates in response to varied Arabidopsis immunities. Model-corrected lesion area means were estimated for three Arabidopsis genotypes at 72-hours post-infection with 96 B. cinerea isolates. The three Arabidopsis genotypes are labeled next to the confidence ellipse curves: wild-type Col-0 (purple dot), jasmonate insensitive mutant coi1-1 (green triangle), and salicylic acid mutant nor1-1 (orange diamond). The 90% confidence ellipse intervals are plotted for each Arabidopsis genotype for reference. Linear regression lines: Col-0: y = 3.2532x + 4.4323, P = 1.008e-10, Adjusted R² = 3.3537; coi1-1: y = 7.4802x + 10.3289, P = 7.895e-15, adjusted R² = 0.4700; npr1-1: y = 3.7086x + 7.3487, P = 2.425e-11, adjusted R² = 0.3726. (E) and (F) Bar plots compare expression variation of BcBOA6 in botcinic acid (BOA) pathway and Bcin01g11460. in cyclic peptide pathway across 96 B. cinerea isolates in response to Arabidopsis wild-type Col-0 immunity. (G) Venn diagram illustrates the number of B. cinerea isolates with the ability to induce BOT, BOA, and cyclic peptide.

cyclic peptide biosynthesis and may represent a novel secondary metabolic pathway in *B*.

277 cinerea (Figure 5-source data 1). The expression of these pathways in planta was extremely

278 variable among the isolates and included some apparent natural knockouts in the expression of

the entire biosynthetic pathway (Figure 6G and Figure 2-source data 1). Isolate 94.4 was the sole

280 genotype lacking the entire BOT pathway, while 19 isolates and 24 isolates did not transcribe

respectively the BOA and the putative cyclic peptide pathways (Figure 6E to 6G and Figure 2-

source data 1). We decomposed the expression of these pathways into expression vectors,

referred to as eigengenes, using a principle component analysis and used a linear mixed model to

test for a relationship between early expression of secondary metabolic pathways and later lesion

area. This showed a significant relationship between the expression of BOT and BOA pathways

and lesion area measured at 72HPI (Supplementary File 2). In contrast, the putative cyclic

287 peptide pathway was only associated with lesion development in a BOT-dependent manner,

suggesting that it may have a synergism to BOT (Supplementary File 2). Thus, in planta analysis

of the fungal transcriptome can identify known and novel potential virulence mechanisms and

associate them with the resulting virulence.

275

291 Covariation of Fungal Virulence Networks Under Differing Plant Immune Responses

292 The *B. cinerea* GCNs measured within Arabidopsis WT provide a reference to investigate how 293 phytohormone-signaling in host innate immunity may shape the pathogen's transcriptional 294 responses during infection. Comparing the *B. cinerea* GCN membership and structure across the 295 three Arabidopsis genotypes (WT, coil-1, and npr1-1) showed that the core membership within 296 networks was largely maintained but the specific linkages within and between GCNs were often 297 variable (Figure 7, Supplementary File 1, Figure 7-figure supplemental 1, 2, 3, and Figure 5-298 source data 1). For example, the two largest B. cinerea GCNs in WT developed multiple co-299 expression connections during infection in the JA-compromised *coil-1* host (Figure 7 and 300 Supplementary File 1). In contrast, some GCNs have a highly robust structure across three host 301 genotypes, including three GCNs associated with BOT, BOA and cyclic peptide production, and 302 GCNs associated with exocytosis regulation, copper transport, and peptidase activity 303 (Supplementary File 1, Figure 7-figure supplemental 1, 2, 3, and Figure 5-source data 1). In 304 addition, we also identified additional small GCNs that demonstrated host specificity in *coil-1* 305 (Figure 7-figure supplemental 2 and Figure 5-source data 1). In particular, there were four small 306 GCNs that are associated with plant cell wall degradation, siderophores, glycolysis, ROS, and S-307 adenosylmethionine biosynthesis (Figure 7-figure supplemental 2). Thus, the coordinated 308 transcriptional responses of *B. cinerea* GCNs are at least partially dependent on variation in the 309 host immune response.

310 Host immunities showed different impacts on expression profiles of genes condensed in

311 individual *B. cinerea* GCNs (Figure 7-figure supplemental 4). Compared with WT, expression

312 profiles of genes within the largest membrane/vesicle virulence GCN were elevated in the SA-

313 and JA-compromised Arabidopsis mutants on average (Figure 7-figure supplemental 4A). 314 Fungal genes associated with copper transport and polyketide production were upregulated under 315 SA-compromised host immunity (Figure 7-figure supplemental 4F and 4J). Whereas, members 316 of GCNs responsible for plant cell wall degradation and siderophore biosynthesis were 317 upregulated under JA-compromised host immunity (Figure 7-figure supplemental 4K and 4L). 318 Finally, GCNs associated with BOT and exocytosis regulation showed robust gene expression 319 profiles across all three Arabidopsis genotypes (Figure 7-figure supplemental 4D and 4G). The 320 above observation indicates host immunity influences the B. cinerea transcriptional response of

321 *B. cinerea* and suggests that *B. cinerea* isolates have varied abilities to tailor virulence strategy in

322 response to host immunity.

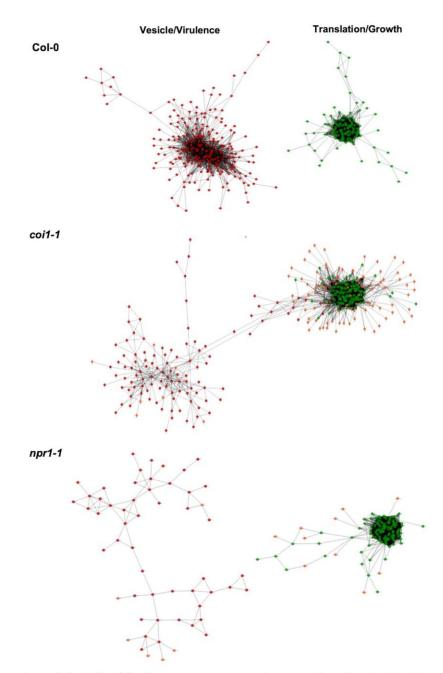
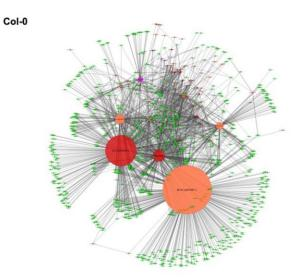


Figure 7. Comparison of plasticity of *B. cinerea* **gene co-expression network under vaired host immunity.** *B. cinerea* gene co-expression networks (GCNs) of vesicle/virulence (red) and translation/growth (green) identified under three Arabidopsis genotypes are compared. Three Arabidopsis genotypes are wild-type Col-0, jasmonate insensitive mutant coi1-1, and salicylic acid mutant *npr1-1*. Nodes marked with red and green colors represent *B. cinerea* genes condensed in GCNs with different biological functions. The same node condensed in GCNs across three Arabidopsis genotypes was marked with same color. Nodes specifically condensed in GCNs under two mutants coi1-1 and *npr1-1* background are marked with orange color. Edges represent the Spearman's rank correlation coefficients between gene pairs.

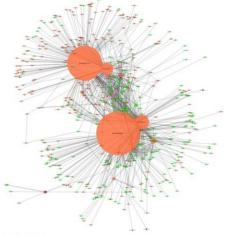
324 Cross-kingdom Co-transcriptomic Networks Revealed Direct Gene-for-gene Interaction

325 To test the interaction between individual genes from two organisms, we generated Arabidopsis-326 B. cinerea GCNs using co-transcriptome data under each host genotype. We calculated 327 Spearman's rank correlation coefficients among 23,898 Arabidopsis transcripts and 9,284 B. 328 cinerea transcripts. This approach identified three cross-kingdom GCNs (CKGCNs) under 329 Arabidopsis WT and JA- or SA-compromised two mutants (Figure 8, Supplementary File 5, and 330 Figure 8-source data 1). Under Arabidopsis WT, a total of 54 hub genes were identified, half 331 from *B. cinerea* and half from Arabidopsis. Furthermore, CKGCNs contain a majority of genes 332 in the BOT GCN and a small proportion of genes in the vesicle/virulence GCN (Figure 8-figure 333 supplemental 1C). For plants, CKGCNs contain a majority of genes from Arabidopsis 334 Defense/camalexin GCN (Figure 8-figure supplemental 1B). These CKGCNs also contain genes 335 associated with extensive host defense responses, i.e., genes encoding membrane-localized 336 leucine-rich repeat receptor kinases (LRR-RKs), stress signal sensing and transduction, 337 tryptophan-derived phytoalexin production, regulation of cell death, cell wall integrity, nutrition 338 transporters, etc. (Figure 8-source data 1). The topological structure and gene content of the 339 CKGCNs shifted across the three Arabidopsis genotypes (Figure 8). These changes illustrate 340 how the host genotype can influence the intercommunication in the host-pathogen interaction.



B coi1-1

Α



71111

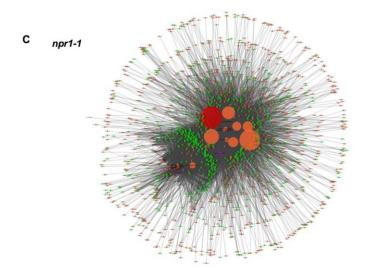


Figure 8. Cross-kingdom Arabidopsis-*B. cinerea* **gene co-expression networks.** Three Arabidopsis genotypes are wildtype Col-0, jasmonate insensitive mutant *coi1-1*, and salicylic acid insensitive mutant *npr1-1*. Green nodes represent Arabidopsis genes. Orange, red and violet nodes represent *B. cinerea* genes. Nodes with red and violet colors are condensed in *B. cinerea* vesicle/virulence and BOT gene co-expression networks, respectively. The degree of a node is shown by the size of a node. Edges represent the Spearman's rank correlation coefficients between gene pairs.

342

343 A Dual Interaction Network Reveals Fungal Virulence Components Targeting Host

344 Immunity

345 To begin assessing how two species influence each other's gene expression during infection, we 346 constructed a co-transcriptome network using both the host- and pathogen-derived GCNs (Figure 347 9 and Figure 9-figure supplemental 1). We converted the ten *B. cinerea* GCNs and the four 348 Arabidopsis GCNs into eigengene vectors that capture the variation of the general expression of 349 all genes within a GCN into a single value (Zhang et al., 2017). The Arabidopsis GCNs were 350 defined in response to this same transcriptome but by using solely the host transcripts. Of these 351 four Arabidopsis GCNs, one is largely comprised of genes in Defense/camalexin signaling, two 352 are linked to different aspects of photosynthesis and the fourth is largely comprised of host genes 353 in cell division. We calculated Spearman's rank coefficients among each GCN eigengene pairs 354 without regard for the species. In this dual transcriptome network, the Arabidopsis/B. cinerea 355 GCN eigengenes are displayed as nodes and positive/negative correlations between the GCNs as 356 edges (Figure 9 and Figure 9-figure supplemental 1). Of the host-derived GCNs, the Arabidopsis 357 Defense/camalexin and Photosystem I (PSI) GCNs have a higher degree of centrality than do the 358 Cell Division or Plastid GCNs across all three host genotypes, suggesting that they have the most 359 interactions with B. cinerea GCNs. In contrast, the fungal GCNs' centrality was more dependent 360 on the host genotype. In WT Col-0, the highest degrees were associated with the exocytosis 361 regulation, BOT, and IPP, whereas they were more peripheral or even not present in the co-362 transcriptome network in the *npr1-1* or *coi1-1* host genotypes. Interestingly, in the WT Col-0

363	host fungal GCNs (Copper transport, Exocytosis regulation, BOT and IPP biosynthesis) that
364	were positively correlated with the host Defense/camalexin GCN showed negative correlations
365	with PSI eigengene. However, the host genotype can change these GCN relationships. In the
366	npr1-1 host, the host Defense/camalexin and PSI GCNs shift to a positive correlation. This may
367	reflect a shift in how the B. cinerea BOT GCN has a positive correlation with the
368	Defense/camalexin GCN in the Col-0 host but a negative correlation in the <i>npr1-1</i> host genotype.
369	This suggests that there are dynamics in the host-pathogen co-transcriptome that can be
370	interrogated to potentially identify causational relationships.
371	To test if these connections were dependent upon the host immunity, we used the eigengene
372	values derived from fungal GCNs to conduct mixed linear modelling of how they were linked to
373	variation in the host genotype and/or host GCNs (Supplementary File 3 and 4). Some B. cinerea
374	GCNs (Vesicle/virulence and TSL/growth, etc.) were more affected by variation in the host
375	genotypes while others had less host dependency on their expression (BOT, Copper transport,
376	etc.). Collectively, pathogen virulence and host immunity GCNs showed complex connections
377	within dual interaction network identified from co-transcriptome data, suggesting functional
378	relationships between host defense and pathogen virulence mechanisms for future
379	experimentation.

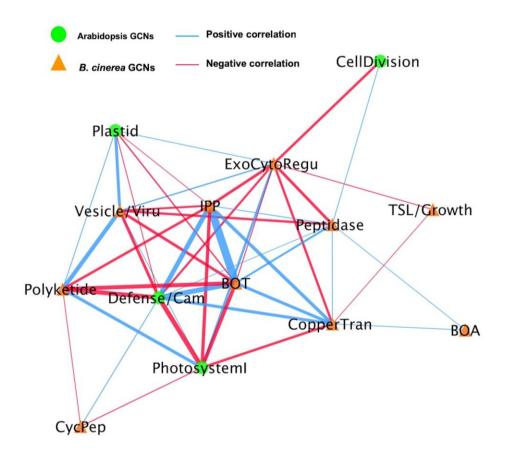


Figure 9. A dual interaction network reveals links between Arabidopsis immunity and *B. cinerea* **virulence.** A dual interaction network was constructed using gene co-expression networks (GCNs) from Arabidopsis and *B. cinerea* co-transcriptome. The first eigenvectors were derived from individual GCNs and used as input to calculate Spearman's rank correlation coefficiency between GCN pairs. Green dots and orange triangles represent Arabidopsis immune- and *B. cinerea* virulence-GCNs, respectively. Blue and red lines (edges) represent the positive and negative Spearman's rank correlation coefficients between GCN pairs, respectively. The thickness of line signifies the correlational strength.

380

381 Germinations Influence on the Co-Transcriptome

- 382 One potential complicating factor that may influence the co-transcriptome is variation in
- 383 germination of the spores between *B. cinerea* strains. The lack of universal genomic patterns for
- 384 host x pathogen interactions in the co-transcriptome argues that germination is not causing global
- 385 effects on the co-transcriptome (Figures 3 and 4). To begin examining how variation in *B*.
- 386 *cinerea* spore germination may influence the co-transcriptome and our identified link to

387 virulence, we investigated the germination of 19 isolates. This showed that there was some 388 variation in germination with all but a few isolates germinating within the 6-7 hours' time frame 389 at room temperature (Figure 9-figure supplemental 2). To extend this to an *in planta* analysis, we 390 utilized an existing microarray study on B. cinerea germination to develop an eigengene that 391 estimates the relative germination between the strains using the *in planta* transcriptomic data 392 (Leroch et al., 2013). We then used this *in planta* estimation of germination to test if our 393 previously identified co-transcriptome to virulence links were altered by controlling for 394 germination. Using linear models, we ran the same test whereby the major *B. cinerea* GCNs 395 were tested for a link to virulence although this time, we included the germination eigengene as a 396 co-variate. This analysis showed that the *in planta* estimation of germination significantly 397 associated with virulence. Critically, even with germination taken into account, all the B. cinerea 398 networks remained significantly associated to lesion area. Some GCNs link, i.e. BOT and BOA, 399 were largely unaffected by the germination estimates (Supplementary File 6), showing that some 400 aspects of virulence are independent of spore germination. In contrast other GCNs like the 401 vesicle linked GCN had their link to virulence decreased but not abolished by including the 402 germination co-variate. Thus, while spore germination plays a role in our measurement of the 403 plant-pathogen interaction, it is only one of multiple factors influencing the co-transcriptome and 404 is not imparting a dominant global influence on the observed patterns.

405 **DISCUSSION**

In recent decades, improvements in the understanding of the molecular basis of plant-pathogen
dynamics have facilitated breeding strategies for disease resistance in a variety of crop species.
However, breeding for disease resistance remains difficult for crops susceptible to pathogens that

409 harbor diverse polygenic virulence strategies targeting multiple layers and components of the 410 plant innate immune system (Corwin and Kliebenstein, 2017). In this study, a co-transcriptomic 411 approach was used to investigat the transcriptome profiles of both fungal pathogen B. cinerea 412 and plant host Arabidopsis at an early infection stage. The results showed that the transcriptional 413 virulence strategy employed by *B. cinerea* is dependent both on fungal genotype and the 414 functional response of the host plant's immune system. A set of *B. cinerea* transcripts were 415 identified with earlier expression associated with later lesion development. Furthermore, ten 416 pathogen GCNs were found responsible for mediating virulence in *B. cinerea*, including a 417 potential specialized metabolic pathway of cyclic peptide virulence factor. Co-transcriptome 418 networks constructed using both plant and pathogen transcriptomic data revealed known and 419 novel fungal virulence components coordinated expressed with plant host GCNs during 420 infection.

421 There are some potential limitations on the utility of cross-species GCNs. Predominantly, they 422 are a correlational approach where links are made between host and pathogen transcriptional 423 changes. While this leads to the development of new hypothesis, it will equally require future 424 validation efforts to assess if these are direct or indirect relationships. Additionally, the cross-425 species GCN approach as implemented in this work does not distinguish between host/pathogen 426 cells that are directly interacting versus those that are having long-distance responses. An 427 important future avenue will be to integrate cell-specific RNA sequencing approaches to better 428 delineate what are the responses within host/pathogen cells that are directly interacting versus the 429 long-distance responses. This would greatly increase the power of elucidating direct versus 430 indirect effects in this system.

431 Secondary Metabolites May Mediate Plant and Fungus Transcriptomic Interactions 432 During Infection

433 Necrotrophic pathogen B. cinerea has evolved an arsenal of virulence strategies to establish 434 colonization and enhance infection within the plant host, including production of secondary 435 metabolites. The co-transcriptome approach shows that the expression of fungal specialized 436 pathways early in infection correlates with later lesion development (Supplementary File 3). 437 Three secondary metabolite GCNs are clustered within the fungal genome and two of them 438 identified with pathway-specific transcription factors (Figure 6, Figure 5, Figure 5-figure 439 supplemental 1, and Figure 5-source data 1). Further, the expression of these pathways displayed 440 a large range of phenotypic variation across the isolates (Figure 6G and Figure 2-source data 1). 441 However, the topology and memberships of GCNs for the three pathways are largely insensitive 442 to variation in host immunity. Robustness to host immunity suggests that these GCNs are 443 somehow insulated from the host's immune response, possibly to protect toxin production from a 444 host counter-attack. The co-transcriptome approach showed the ability to identify known and 445 novel secondary metabolic pathways that mediate plant host and fungal pathogen interaction.

Importantly, the dual interaction networks provide hypothesis for pathogen-GCNs responsible for fungal secondary metabolites production link to specific plant host-GCNs (Figure 9 and Figure 9-figure supplemental 1). Specifically, the co-transcriptome approach revealed that *B. cinerea* GCNs responsible for secondary metabolite production are associated with both plant immune responses and primary plant metabolism (Figure 9, Figure 9-figure supplemental 1, Supplementary File 3 and 4). For example, in the WT Col-0 host genotype the BOT GCN shows a strong positive correlation with the Arabidopsis Defense/camalexin GCN, suggesting that BOT

453 production may directly induce the host's defense system. Concurrently, the BOT GCN is 454 negatively linked to the plant's PSI GCN, suggesting that BOT may repress the plant's 455 photosynthetic potential. Critically, this relationship changes in the *npr1-1* host genotype with 456 the BOT GCN now having a negative correlation to the Arabidopsis Defense/camalexin GCN. 457 Further work is needed to test if these host/pathogen GCN interactions are causal and how the 458 SA pathway in the host may influence these interactions. Collectively, these results strongly 459 implicate the ability of secondary metabolites biosynthesis to mediate the interactions between 460 pathogen virulence and plant host immunity at the transcriptomic level. The co-transcriptome 461 approach showed the potential to enable us to form new hypotheses about how this linkage may 462 occur.

463 Fungal Virulence Components Correlated with Plant Immune Response

464 In addition to secondary metabolite biosynthesis, the co-transcriptome identified a number of key 465 virulence mechanisms that could be mapped to the two species interaction. One key GCN is 466 enriched for genes involved in exocytosis associated regulation (Figure 5-Exocytosis regulation 467 and Figure 5-source data 1). The exocytosis complex is responsible for delivery of secondary 468 metabolites and proteins to the extra-cellular space and plasma membrane in fungi (Colombo et 469 al., 2014; Rodrigues et al., 2015). Additionally, we found many B. cinerea genes associated 470 with secretory vesicles within the membrane/vesicle virulence GCN that likely serve a similar 471 function during infection (Figure 5-Vesicle/virulence and Figure 5-source data 1). These GCNs 472 also provide support for the role of exocytosis-based spatial segregation of different materials 473 during fungal hyphae growth *in planta* (Samuel et al., 2015). The dual interaction network 474 suggests that the exocytosis regulation and membrane/vesicle virulence GCNs are differentially

475 linked to the Arabidopsis Defense/camalexin GCN, indicating varied connections between 476 fungal secretory pathways and plant immune responses (Figure 9 and Supplementary File 3 and 477 4). Another conserved GCN in the *B. cinerea* species is associated with copper uptake and 478 transport (Figure 5-Copper transport, Figure 7-figure supplemental 1, 2, 3, and Figure 5-source 479 data 1). Although copper is essential for *B. cinerea* penetration and redox status regulation within 480 plant tissues, further work is required to decipher the precise molecular mechanism involved in 481 acquisition and detoxification of copper. Thus, the co-transcriptome approach can identify both 482 known and unknown mechanisms and links within the host-pathogen interaction.

483 Fungal Virulence Transcriptomic Responses Are Partly Shaped by Host Immunity

484 It is largely unknown how plant host immunity contributes to the transcriptomic behavior of the 485 fungus during infection. Even less is known about the role of genetic variation in the pathogen in responding to, or coping with, the inputs coming from the host immune system. In the current 486 487 study, we found that the host immune system's effect on pathogen transcripts and GCNs was 488 largely via an interaction with the pathogens genotype (Figure 2, Figure 7, Figure 7-figure 489 supplemental 4, and Figure 2-source data 4). For example, fungal GCNs associated with 490 membrane/vesicle virulence and fungal growth shifted drastically between the WT and coil-1 or 491 *npr1-1* Arabidopsis genotypes (Figure 7). In addition, some GCNs only appeared in specific 492 backgrounds. For example, those linked to siderophores and a polyketide production were only 493 identified during infection of the JA-compromised Arabidopsis mutant (Figure 7-figure 494 supplemental 4J and 4L). However, other fungal GCNs, like those involved in secondary 495 metabolism, were largely insensitive to variation in the host immunity (Figure 7-figure 496 supplemental 1, 2, 3, Supplementary File 1, and Figure 5-source data 1). Critically, the gene

membership of these GCNs is largely stable across the collection of pathogen isolates, even
while their expression level across the *B. cinerea* isolates is highly polymorphic (Figure 5-source
data 1 and Figure 7-figure supplemental 4). This suggests that natural variation in the host
immunity and pathogen shapes how the co-transcriptome responds to host's immune system.
Further, the natural variation in the pathogen may be focused around these functional GCNs.

502 Plant Disease Development Can Be Predicted by Early Transcriptome Data

503 Plant disease development is an abstract phenomenon that is the result of a wide set of 504 spatiotemporal biological processes encoded by two interplaying species under a specific 505 environment. In current study, we used late stage lesion area as a quantitative indicator of B. 506 *cinerea* virulence. We have previously shown that early Arabidopsis transcriptomic response 507 could be linked to later lesion development (Zhang et al., 2017). Here, our findings suggest that 508 the late-stage disease development of a *B. cinerea* infection is determined during the first few 509 hours of infection by the interaction of plant immune and fungal virulence responses. It was 510 possible to create a link between early transcripts' accumulation and late disease development 511 using solely the *B. cinerea* transcriptome (Figure 1 and Figure 3-source data 1). This could be 512 done using either individual pathogen genes, GCNs, or more simply the total fraction of 513 transcripts from the pathogen. As the transcriptomic data were from plant leaf tissue only 16HPI, 514 there is not a significant amount of pathogen biomass and this is more likely an indicator of 515 transcriptional activity in the pathogen during infection. It is possible to develop these methods 516 as possible biomarkers for likely fungal pathogen caused disease progression.

517 CONCLUSION

518 The co-transcriptome analysis of a *B. cinerea* population infection on Arabidopsis identified a 519 number of B. cinerea GCNs that contained a variety of virulence-associated gene modules with 520 different biological functions. The characterization of these GCNs simultaneously identified 521 mechanisms known to enhance B. cinerea virulence and implicated several novel mechanisms 522 not previously described in the Arabidopsis-B. cinerea pathosystem. In addition, the plant-fungus 523 co-transcriptome network revealed the potential interaction between fungal pathogen- and plant 524 host-GCNs. Construction of GCNs within single species, CKGCNs and dual networks shed 525 lights on the biological mechanisms driving quantitative pathogen virulence in *B. cinerea* and 526 their potential targets in the plant innate immune system.

527 METHODS

528 Collection and Maintenance *B. cinerea* Isolates

529 A collection of 96 B. cinerea isolates were selected in this study based on their phenotypic and 530 genotypic diversity (Denby et al., 2004; Rowe and Kliebenstein, 2007; Corwin et al., 2016; 531 Zhang et al., 2016; Zhang et al., 2017). This B. cinerea collection was sampled from a large 532 variety of different host origins and contained a set of international isolates obtained from labs 533 across the world, including the well-studied B05.10 isolate. A majority of isolates are natural 534 isolates that isolated from California and can infect a wide range of crops. Isolates are 535 maintained in -80°C freezer stocks as spores in 20% glycerol and were grown on fresh potato 536 dextrose agar (PDA) 10 days prior to infection.

537 Plant Materials and Growth Conditions

538 The Arabidopsis accession Columbia-0 (Col-0) was the wildtype background of all Arabidopsis 539 mutants used in this study. The three Arabidopsis genotypes used in this study included the WT 540 and two well-characterized immunodeficient mutants, *coil-1* and *npr1-1*, that abolish the major 541 JA- or SA-defense perception pathways, respectively (Cao et al., 1997; Xie et al., 1998; Xu, L. 542 et al., 2002; Pieterse and Van Loon, 2004). All plants were grown as described previously 543 (Zhang et al., 2017). Two independent randomized complete block-designed experiments were 544 conducted and a total of 90 plants per genotype were grown in 30 flats for each experiment. 545 Approximately 5 to 6 fully developed leaves were harvested from the five-week old plants and 546 placed on 1% phytoagar in large plastic flats prior to B. cinerea infection.

547 Inoculation and Sampling

548 We infected all 96 isolates onto each of the three Arabidopsis genotypes in a random design with 549 6-fold replication across the two independent experiments. A total of twelve infected leaves per 550 isolate/genotype pair were generated. For inoculation, all *B. cinerea* isolates were cultured and 551 inoculated on three Arabidopsis genotypes as described previously (Denby et al., 2004; Corwin 552 et al., 2016; Zhang et al., 2017). Briefly, frozen glycerol stocks of isolate spores were first used 553 for inoculation on a few slices of canned peaches in petri plates. Spores were collected from one-554 week-old sporulating peach slices. The spore solution was filterred and the spore pellet was re-555 suspended in sterilized 0.5x organic grape juice (Santa Cruz Organics, Pescadero, CA). Spore 556 concentrations were determined using a hemacytometer and suspensions were diluted to 557 10spores/µL. Detached leaf assays were used for a high-throughput analysis of B. cinerea 558 infection, which has been shown to be consistent with whole plant assay (Govrin and Levine, 559 2000; Mengiste et al., 2003; Denby et al., 2004; Sharma et al., 2005; Windram et al., 2012).

Five-week old leaves were inoculated with 4μL of the spore solution. The infected leaf tissues were incubated on 1% phytoagar flats with a humidity dome at room temperature. The inoculation was conducted in a randomized complete block design across the six planting blocks. All inoculations were conducted within one hour of dawn and the light period of the leaves was maintained. Two blocks were harvest at 16HPI for RNA-Seq analysis. The remaining four blocks were incubated at room temperature until 72HPI when they were digitally imaged for lesion size and harvested for chemical analysis as described previously (Zhang et al., 2017).

567 RNA-Seq Library Preparation, Sequencing, Mapping and Statistical Analysis

568 Two B. cinerea infected leaf tissues of the six blocks were sampled at 16HPI for transcriptome 569 analysis, which resulted in a total of 1,052 mRNA libraries for Illumina HiSeq sequencing. 570 RNA-Seq libraries were prepared according to a previous method (Kumar et al., 2012) with 571 minor modifications (Zhang et al., 2017). Briefly, infected leaves were immediately frozen in 572 liquid nitrogen and stored at -80°C until processing. RNA extraction was conducted by re-573 freezing samples in liquid nitrogen and homogenizing by rapid agitation in a bead beater 574 followed by direct mRNA isolation using the Dynabeads oligo-dT kit. First and second strand 575 cDNA was produced from the mRNA using an Invitrogen Superscript III kit. The resulting 576 cDNA was fragmented, end-repaired, A-tailed and barcoded as previously described. Adapter-577 ligated fragments were enriched by PCR and size-selected for a mean of 300 base pair (bp) prior 578 to sequencing. Barcoded libraries were pooled in batches of 96 and submitted for a single-end, 579 50bp sequencing on a single lane per pool using the Illumina HiSeq 2500 platform at the UC 580 Davis Genome Center (DNA Technologies Core, Davis, CA).

581 Transcriptomic Data Analysis

582 Fastq files from individual HiSeq lanes were separated by adapter index into individual RNA-

Seq library samples. The quality of individual libraries was estimated for overall read quality and
over-represented sequences using FastQC software (Version 0.11.3,

585 www.bioinformatics.babraham.ac.uk/projects/). We conducted downstream bioinformatic

analysis, like reads mapping, normalization and nbGLM model analysis, using a custom script

from the Octopus R package (https://github.com/WeiZhang317/octopus). The mapping of

588 processed reads against Arabidopsis and *B. cinerea* reference genomes was conducted by Bowtie

589 1 (V.1.1.2, http://sourceforge.net/projects/bowtie-bio/files/bowtie/1.1.2/) using minimum

590 phred33 quality scores (Langmead et al., 2009). The first 10bp of reads was trimmed to remove

591 low quality bases using the fastx toolkit

592 (http://hannonlab.cshl.edu/fastx_toolkit/commandline.html). Total reads for each library were

593 firstly mapped against the Arabidopsis TAIR10.25 cDNA reference genome. The remaining un-

594 mapped reads were then aligned against *B. cinerea* B05.10 isolate cDNA reference genome

595 (Lamesch et al., 2010; Lamesch et al., 2012; Krishnakumar et al., 2015; Van Kan et al., 2017)

and the gene counts for both species were pulled from the resulting SAM files (Li et al., 2009).

597 For pathogen gene expression analysis, we first filtered genes with either more than 30 gene

counts in one isolate or 300 gene counts across 96 isolates. We normalized *B. cinerea* gene

599 counts data set using the trimmed mean of M-values method (TMM) from the EdgeR package

600 (V3.12) (Robinson and Smyth, 2008; Bullard et al., 2010; Robinson and Oshlack, 2010). We

then ran the following generalized linear model (GLM) with a negative binomial link function

from the MASS package for all transcripts using the following equation (Venables and Ripley,

603 **2002**):

604 $Y_{egai} = E_e + E_e(Gf_g) + E_e(Gf_g(Af_a)) + I_i + H_h + H_h^* I_i$

605 where the main categorical effects E, I, and H are denoted as experiment, isolate genotype, and 606 plant host genotype, respectively. Nested effects of the growing flat (Gf) within the experimental 607 replicates and agar flat (Af) nested within growing flat are also accounted for within the model. 608 Model corrected means and standard errors for each transcript were determined for each 609 isolate/plant genotype pair using the lsmeans package (Russell V. Lenth, 2016). Raw P-values 610 for F- and Chi Square-test were determined using Type II sums of squares using *car* package 611 (Fox and Weisberg, 2011). *P*-values were corrected for multiple testing using a false discovery rate correction (Benjamini Yoav and Yekutieli Daniel, 2001). Broad-sense heritability (H^2) of 612 613 individual transcripts was estimated as the proportion of variance attributed to B. cinerea 614 genotype, Arabidopsis genotype, or their interaction effects.

615 Gene Ontology Analysis

616 GO analysis was conducted for several *B. cinerea* gene sets that were identified with high heritability,

617 correlated with lesion size, and condensed in network analysis. We first converted sequences of these *B*.

618 *cinerea* genes into fasta files using *Biostrings* and *seqRFLP* packages in R (Ding Qiong and Zhang

519 Jinlong, 2012; Pages et al., 2017). The functional annotation of genes was obtained by blasting the

620 sequences against the NCBI database using Blast2GO to obtain putative GO annotations (Conesa et al.,

621 2005; Gotz et al., 2008). The GO terms were compared to the official GO annotation from the *B*.

622 *cinerea* database (<u>http://fungi.ensembl.org/Botrytis_cinerea/Info/Index</u>) and those obtained by Blast2GO

623 analysis. The official gene annotations for host genes was retrieved from TAIR10.25

624 (<u>https://apps.araport.org/thalemine/bag.do?subtab=upload</u>).

625 B. cinerea Gene Co-expression Network Construction

626 To obtain a representative subset of *B. cinerea* genes co-expressed under *in planta* conditions, 627 we generated gene co-expression networks (GCNs) among genes in the *B. cinerea* transcriptome. 628 GCNs were generated using the model-corrected means of 9,284 B. cinerea transcripts from 629 individual isolate infection across three Arabidopsis genotypes. Only genes with average or 630 medium expression greater than zero across all samples were considered. This preselection 631 process kept 6,372 genes and those with negative expression values were adjusted to set 632 expression at zero before network construction. Spearman's rank correlation coefficients for each 633 gene pair was calculated using the *cor* function in R. Three gene-for-gene correlation similarity 634 matrixes were generated independently for each of the three Arabidopsis genotypes. Considering 635 the cutoff for gene-pair correlation usually generates biases of GCN structure and the candidate 636 gene hit, we utilized several cutoff threshold values at 0.75, 0.8, 0.85, and 0.9 to filter the gene 637 set. Comparing the structure and content of GCNs among those GCN sets using filtered gene set 638 as input, we selected the correlation threshold at 0.8. A total of 600, 700 and 494 B. cinerea 639 candidate genes passed the criterion under Arabidopsis WT, mutants *coil-1* and *npr1-1*, 640 respectively. To obtain a representative subset of *B. cinerea* gene candidates across three host 641 genotypes, we selected gene candidates that presented across the above three gene subsets. This process generated a gene set with 323 B. cinerea candidate genes that were common to each of 642 643 the plant genotype backgrounds and had at least 0.8 significant correlations. Using this gene set 644 as kernel, we extended gene candidate sets under each Arabidopsis genotype. The expanded B. 645 *cinerea* gene candidate set under individual Arabidopsis genotypes was further used as input for 646 gene co-expression network construction.

647 GCNs were visualized using Cytoscape V3.2.1 (Java version:1.8.0_60) (Shannon et al., 2003).
648 The nodes and edges within each network represent the *B. cinerea* genes and the Spearman's

rank correlations between each gene pair. The importance of a given node within each network was determined by common network analysis indices, such as connectivity (degree) and betweenness. Nodes with higher connectivity and betweenness were considered as hub and bottleneck genes, respectively, and the biological functions of each network were determined by the GO terms of hub and bottle neck genes using Blast2GO.

654 Cross-kingdom Arabidopsis-B. cinerea Gene Co-expression Network Construction

655 We used model-corrected means of transcripts from three Arabidopsis host genotypes and 96 B.

656 cinerea isolates to construct the cross-kingdom Arabidopsis-B. cinerea GCNs. Model-corrected

657 means of 23,959 Arabidopsis transcripts and 6,372 *B. cinerea* transcripts derived from two

negative binomial linked generalized linear models were served as input data sets (Zhang et al.,

659 2017). Spearman's rank correlation coefficient was calculated between genes from Arabidopsis

and *B. cinerea* data sets. The gene pairs with positive correlations greater than 0.74 under each

661 Arabidopsis genotype were considered to construct cross-kingdom GCNs.

662 **Dual Interaction Network Construction**

To construct a cross-kingdom, dual interaction network of plant-pathogen GCNs, we performed principle component analysis on individual GCNs within each species to obtain eigengene vectors describing the expression of the entire gene network as previously described (Zhang and Horvath, 2005; Langfelder and Horvath, 2008; Okada et al., 2016). From these eigengene vectors, we calculated the Spearman's rank correlation coefficient between the first eigengene vectors for each network. The resulting similarity matrices were used as input to construct the interaction network and Cytoscape was used to visualize the resulting network.

670 Statistical Analysis of Network Components

671 All the analyses were conducted using R V3.2.1 statistical environment (R Core Team, 2014). To 672 investigate how secondary metabolite induction in *B. cinerea* contributes to disease 673 development, we conducted a multi-factor ANOVA on *B. cinerea* three secondary metabolic 674 pathways upon impacts on host genotypes. The three secondary metabolic pathways included the 675 biosynthetic pathways of two well-known secondary metabolites, BOT and BOA, and a cyclic 676 peptide biosynthetic pathway predicted in this study. We calculated the z-scores for all 677 transcripts involved in BOT pathway, the BOA, and the putative cyclic peptide pathway for each 678 isolate/plant genotype pair. The multi-factor ANOVA model for lesion area was: $y_{Lesion} = \mu + T * A * C * G_h + \varepsilon$ 679 680 where T, A, C, and G_b stand for BOT, BOA, Cyclic peptide, and host genotype, respectively. 681 In addition, we used multi-factor ANOVA models to investigate interactions between GCNs 682 within species for impacts upon host genotypes. The ANOVA models contain all GCNs within a 683 species. The first eigengene vector derived from principal component analysis on each network 684 was used in ANOVA models. The ANOVA model for individual *B. cinerea* GCNs was: $y_{BcNeti} = \mu + D * P * C * PSI * G_h + \epsilon$ 685 686 where D, P, C, PSI, and G_h stand for Arabidopsis Defense/Camalexin GCN, Arabidopsis Plastid 687 GCN, Arabidopsis Cell/Division GCN, Arabidopsis PSI GCN, and Host genotypes, respectively. 688 G_h stands for HostGenotype, respectively. BcNeti represents one of the ten B. cinerea GCNs 689 identified in this study. The ANOVA model for individual Arabidopsis GCNs was:

690 $y_{AtNeti} = \mu + \sum BcNeti + G_h + \varepsilon$

691	where \sum BcNeti represents the summation of each of the ten <i>B</i> . <i>cinerea</i> GCNs identified in this
692	study: BcVesicle/Viru GCN, BcTSL/Growth GCN, BcBOA GCN, BcExocytoRegu GCN,
693	BcCycPep GCN, BcCopperTran GCN, BcBOT GCN, BcPeptidase GCN, BcIPP GCN,
694	BcPolyketide GCN, while G _h stands for Host genotypes. Interactions among the terms were not
695	tested to avoid the potential for overfitting. AtNeti stands for one of the four Arabidopsis GCNs
696	(e.g. AtDefense/Camalexin GCN, AtPlastid GCN, AtCell/Division GCN, AtPSI GCN). All
697	multi-factor ANOVA models were optimized by trimming to just the terms with a significant P-
698	value (<i>P</i> -value < 0.05).

699 Germination Assay

700 To assess the potential for natural variation in germination time in the isolate collection, 19 B. 701 *cinerea* isolates were investigated by germination assay. The isolates were grown on PDA. 702 Mature spores were collected in water, filtered and resuspended in 50% grape juice, as 703 previously described, and further diluted to 1000spores/µL. To prevent germination before the 704 beginning of the assay, spores were continuously kept on ice or in the fridge at 4°C. During the 705 germination assay, the spores were maintained at 21°C in 1.5mL tubes. Every hour, the tubes 706 were mixed by manual inversion and sampled for 25μ L that were transferred to microscope 707 slides. The spores within the drops were let to set down shortly. Without using slide covers, the 708 spores were observed within the drops at two locations, used as technical replicates. The spores 709 were categorized and counted based on the picture of every microscope observations taken every 710 hour from 2 to 11 hours. Germination was defined as the hyphae emerged out of the spore.

To assess the contribution of germination to the observed *B. cinerea* transcriptomic networks
involved in lesion development, we generated germination estimates based on gene expression

713 by extracting the first principal component of a publicly available time series microarray data 714 including 101 gemination-associated genes (Leroch et al., 2013). Based on this principal 715 component, we predicted the level of expression of germination-associated genes for the 96 716 isolates on the three Arabidopsis genotypes at 16HPI. Theses germination predictions for 717 individual isolates were used in a linear ANOVA model to estimate the co-linearity of the 718 germination eigengene vector to virulence. Using linear ANOVA models with and without this 719 germination eigengene vector, we compared how germination influences the 10 B. cinerea 720 transcriptomic networks involved in lesion area in the three host genotypes. The ANOVA 721 models with and without germination eigengene vector were:

722
$$Y_{\text{Lesion}} = \mu + \text{Germination} + \sum BcNeti + G_h + \varepsilon$$

723 $Y_{\text{Lesion}} = \mu + \sum BcNeti + G_h + \varepsilon$

where Germination represents the scores of first principal components on expressions of

germination associated genes from *B. cinerea* transcriptomic data in this study, Σ BcNeti

represents the summation of each of the ten *B. cinerea* GCNs identified in this study:

727 BcVesicle/Viru GCN, BcTSL/Growth GCN, BcBOA GCN, BcExocytoRegu GCN, BcCycPep

728 GCN, BcCopperTran GCN, BcBOT GCN, BcPeptidase GCN, BcIPP GCN, BcPolyketide GCN,

while G_h stands for Host genotypes. Interactions among the terms were not tested to avoid the
 potential for overfitting.

731 Data Availability

The datasets in this study are available in the following database: Bioproject PRJNA473829

733 (https://www.ncbi.nlm.nih.gov/bioproject/?term=PRJNA473829). The computer scripts used in

this study are available in GitHub (https://github.com/WeiZhang317/octopus).

735 Funding

736 Funding for this work was provided by the NSF award IOS 1339125 to DJK, the USDA National 737 Institute of Food and Agriculture, Hatch project number CA-D-PLS-7033-H to DJK and by the 738 Danish National Research Foundation (DNRF99) grant to DJK, the China Scholarship Council 739 grant 20130624 to WZ.

740 **Figure legends**

741

Figure 1. Correlation between earlier estimated *B. cinerea* biomass and later lesion area. 742 Model-corrected lesion area means were estimated using the linear model on the six replicates 743 data from three Arabidopsis genotypes at 72-hours post-infection with 96 B. cinerea isolates. 744 Estimated biomass of *B. cinerea* was calculated using the linear model-corrected fraction of *B.* 745 cinerea mapped reads against total mapped reads to Arabidopsis and B. cinerea reference 746 genomes. RNA-Seq analysis was conducted at 16-hours post-infection for each pathosystem. 747 Three Arabidopsis genotypes are wild-type Col-0 (purple dot), jasmonate insensitive mutant 748 *coil-1* (green triangle), and salicylic acid insensitive mutant *npr1-1* (orange diamond). The 90% 749 confidence ellipse intervals are plotted for each Arabidopsis genotype for references. Quadratic

regression lines are: Col-0: $y = -0.00059x^{2} + 0.729x + 10.037$, P = 0.0016, adjusted $R^{2} = 0.1101$; 750

coil-1: y = -0.117x² + 4.44x - 0.1585, P = 3.914e-07, adjusted R² = 0.2562; npr1-1: y = -751

752
$$0.0579x^2 + 2.26x + 1.673, P = 0.0001$$
, adjusted $R^2 = 0.161$.

753 Figure 2. Transcriptomic responses of *B. cinerea* on Arabidopsis are controlled by genetic

754 variation in pathogen population, host genotypes, and their interaction. (A) Distribution of

- broad-sense heritability (H^2) of *B. cinerea* transcripts contributed by genetic variation in the *B*. 755
- 756 *cinerea*, Arabidopsis genotypes, and the interaction between pathogen and host. Violin plots

757	illustrating the distribution of H^2 for transcripts from 96 <i>B. cinerea</i> isolates infecting on
758	Arabidopsis genotypes. Heritability is partitioned across the different sources, 96 pathogen
759	genotypes = "Isolate", plant genotypes Col-0, <i>coi1-1</i> and <i>npr1-1</i> plant genotypes = "Host", and
760	the corresponding interaction. The transcriptomic analysis was conducted by sequencing mRNA
761	extracted from B. cinerea infected Arabidopsis leaves at 16-hours post-infection. Red lines
762	indicate the average broad-sense heritability values of lesion area caused by isolates, Arabidopsis
763	genotypes, and their interaction. (B) to (E) Expression profiles of B. cinerea transcripts
764	significantly influenced by host genotypes. The model-corrected means (log ₂) for <i>B. cinerea</i>
765	transcript were used for plotting. The Arabidopsis genotypes, wild-type Col-0 (purple),
766	jasmonate insensitive mutant coil-1 (green), and salicylic acid mutant npr1-1 (orange), are
767	shown on the x axis. B. cinerea transcripts are: (B) Bcin01g03790.1, class IV chitin synthase; (C)
768	Bcin02g02980.1, Monooxygenase; (D) Bcin10g02260.1, NADH oxidoreductase; (E)
769	Bcin11g05200.1, caffeine-induced death Cid2; (F) to (I) Expression profiles of B. cinerea
770	transcripts significantly influenced by the interaction between pathogen and host genotypes. (F)
771	Bcin02g03810.1, GTP cyclohydrolase; (G) Bcin09g01190.1, Tripeptidyl-peptidase 1; (H)
772	Bcin10g01130.1, in secretory pathway; (I) Bcin14g05090.1, a transcription factor.

773 Figure 3. Expression profiles of an endopolygalacturonase gene *Bcpg1* from diverse *B*.

774 *cinerea* isolates across Arabidopsis genotypes. Rank plot shows the relationship of *Bcpg1*

expression from 32 diverse *B. cinerea* isolates (right) across three Arabidopsis genotypes (x

- axis). Three Arabidopsis genotypes are wild-type Col-0 (purple dot), jasmonate insensitive
- 777 mutant *coil-1* (green triangle), and salicylic acid mutant *npr1-1* (orange diamond). The model-
- corrected means (log₂) for the transcript of *Bcpg1* (*Bcin14g00850.1*) encoding an
- endopolygalacturonase gene are utilized for plotting. The transcript expression levels from the

same isolate across three Arabidopsis genotypes are connected with a colored line. The names of
32 isolates are represented with the same colored lines as induced *Bcpg1* expression levels.

782 Black lines indicate the expression levels of *Bcpg1* are higher in *coi1-1* and *npr1-1* than in Col-0.

Red lines indicate the higher expression levels of *Bcpg1* in *coi1-1* but lower in *npr1-1*. Blue lines

indicate the highest expression levels of *Bcpg1* are in Col-0. Dark green lines indicate the higher

expression levels of *Bcpg1* in *npr1-1* but lower in *coi1-1*.

786 Figure 4. Interaction effects of host genotypes and pathogen isolates on *B. cinerea*

transcriptome. Hierarchical clustering of relative expression of 500 genes from 96 *B. cinerea* isolates infection on Arabidopsis mutants *coil-1* (A) or *npr1-1* (B) are plotted based on pairwise comparison of pathogen gene expression under Col-0. The 500 *B. cinerea* genes with highest broad-sense heritability (H^2) of host X pathogen were used for analysis. Lesion area induced by 96 isolates are compared under *coil-1* (green bar plot) and *npr1-1* (orange bar plot).

792 Figure 5. Gene co-expression networks identified from *B. cinerea* transcriptomic responses

793 to Arabidopsis wild-type Col-0 immunity. Ten gene co-expression networks (GCNs) with

more than five nodes were identified from 96 B. cinerea isolates infecting on Arabidopsis wild-

type Col-0. The similarity matrix is computed using Spearman's rank correlation coefficient.

796 Nodes with different colors represent *B. cinerea* genes condensed in GCNs with different

biological functions. Edges represent the Spearman's rank correlation coefficients between gene

pairs. Trans- and cis-GCNs means GCNs are regulated by trans- and cis-regulatory elements,

respectively. GCNs were named after their biological functions, which were determined by hub

800 and bottleneck genes within each network. GCNs are: vesicle/virulence (red), translation/growth

801 (green), exocytosis regulation (pink), cyclic peptide (yellow), peptidase (gray), isopentenyl

802 pyrophosphate (IPP, turquoise), polyketide (violet), botcinic acid (BOA, blue), copper transport
803 (slate blue), botrydial (BOT, purple).

804 Figure 6. Variation of transcripts accumulation for secondary metabolites production 805 across diverse B. cinerea isolates. Expression profiles of genes responsible for botrydial, 806 botcinic acid, cyclic peptide production across 96 isolates under Arabidopsis wild-type Col-0 are 807 shown. (A) Schematic shows the genomic locus of seven botrydial (BOT) biosynthesis genes 808 clustered together. Exons are represented by gray boxes. Introns and intergenic regions are 809 represented by the grey line. Seven BOT genes are: *BcBOT1*, *BcBOT3* and *BcBOT4*, encoding a 810 cytochrome P450 monooxygenase, respectively; *BcBOT2* encoding a sesquiterpene cyclase; 811 BcBOT5 encoding an acetyl transferase; BcBOT6 encoding a Zn(II)2Cys6 transcription factor, 812 BcBOT7 encoding a dehydrogenase reductase. (B) BOT biosynthesis pathway in B. cinerea. (C) 813 Bar plots compare expression variation of BcBOT2 across 96 B. cinerea isolates in responding to 814 Arabidopsis wild-type Col-0 immunity. The model-corrected means (log₂) of transcripts were 815 used for plotting. (D) Scatter plot illustrates the positive correlations between lesion area and 816 accumulation of *BcBOT2* transcript across the 96 isolates in response to varied Arabidopsis 817 immunities. Model-corrected lesion area means were estimated for three Arabidopsis genotypes 818 at 72-hours post-infection with 96 B. cinerea isolates. The three Arabidopsis genotypes are 819 labeled next to the confidence ellipse curves: wild-type Col-0 (purple dot), jasmonate insensitive 820 mutant *coi1-1* (green triangle), and salicylic acid mutant *npr1-1* (orange diamond). The 90% 821 confidence ellipse intervals are plotted for each Arabidopsis genotype for reference. Linear regression lines: Col-0: y = 3.2532x + 4.4323, P = 1.008e-10, Adjusted $R^2 = 3.3537$; *coi1-1*: y =822 823 7.4802x + 10.3289, P = 7.895e-15, adjusted $R^2 = 0.4700$; npr1-1: y = 3.7086x + 7.3487, P =2.425e-11, adjusted $R^2 = 0.3726$. (E) and (F) Bar plots compare expression variation of *BcBOA6* 824

in botcinic acid (BOA) pathway and *Bcin01g11460*. in cyclic peptide pathway across 96 *B*. *cinerea* isolates in response to Arabidopsis wild-type Col-0 immunity. (G) Venn diagram
illustrates the number of *B. cinerea* isolates with the ability to induce BOT, BOA, and cyclic
peptide.

829 Figure 7. Comparison of plasticity of *B. cinerea* gene co-expression network under vaired

830 host immunity. B. cinerea gene co-expression networks (GCNs) of vesicle/virulence (red) and

translation/growth (green) identified under three Arabidopsis genotypes are compared. Three

832 Arabidopsis genotypes are wild-type Col-0, jasmonate insensitive mutant *coi1-1*, and salicylic

833 acid mutant npr1-1. Nodes marked with red and green colors represent B. cinerea genes

condensed in GCNs with different biological functions. The same node condensed in GCNs

835 across three Arabidopsis genotypes was marked with same color. Nodes specificaly condensed in

836 GCNs under two mutants *coil-1* and *npr1-1* background are marked with orange color. Edges

837 represent the Spearman's rank correlation coefficients between gene pairs.

838 Figure 8. Cross-kingdom Arabidopsis-B. cinerea gene co-expression networks. Networks 839 showing the co-expression connectivity between Arabidopsis and B. cinerea genes within three 840 Arabidopsis genotypes are shown. (A) shows connectivity within Arabidopsis wild-type Col-0, 841 (B) shows connectivity within the Arabidopsis jasmonate insensitive mutant *coil-1*, and (C) 842 shows connectivity within the Arabidopsis salicylic acid insensitive mutant *npr1-1*. Within each 843 connectivity plot, orange and green nodes show transcripts from *B. cinerea* and Arabidopsis, 844 respectively. Nodes with red and violet colors represent the *B. cinerea* transcripts that were 845 found to be members of the B. cinerea membrane/vesicle virulence network and BOT network,

respectively. Node size shows the number of interactions with a specific gene. The connectivitybetween the nodes was derived using Spearman's rank correlation analysis.

848 Figure 9. A dual interaction network reveals links between Arabidopsis immunity and B. 849 cinerea virulence. A dual interaction network was constructed using gene co-expression 850 networks (GCNs) from Arabidopsis and B. cinerea co-transcriptome. The first eigenvectors were 851 derived from individual GCNs and used as input to calculate Spearman's rank correlation 852 coefficiency between GCN pairs. Green dots and orange triangles represent Arabidopsis 853 immune- and B. cinerea virulence-GCNs, respectively. Blue and red lines (edges) represent the 854 positive and negative Spearman's rank correlation coefficients between GCN pairs, respectively. 855 The thickness of line signifies the correlational strength.

856 Supplemental Data

857 Figure 3-figure supplemental 1. Expression profiles of an oxaloacetate hydrolase gene 858 Bcoah from diverse B. cinerea isolates across Arabidopsis genotypes. Rank plot shows the 859 relationship o Bcoah expression from 32 diverse B. cinerea isolates (right) across three 860 Arabidopsis genotypes (x axis). Three Arabidopsis genotypes are wild-type Col-0 (purple dot), 861 jasmonate insensitive mutant *coil-1* (green triangle), and salicylic acid mutant *npr1-1* (orange 862 diamond). The model-corrected means (log₂) for the transcript of *Bcoah* (*Bcin12g01020.1*) 863 encoding an oxaloacetate hydrolase gene are utilized for plotting. The transcript expression 864 levels from the same isolate across three Arabidopsis genotypes are connected with a colored 865 line. The names of 32 isolates are represented with the same colored lines as induced *Bcoah* 866 expression levels. Black lines indicate the expression levels of *Bcoah* are higher in *coil-1* and 867 npr1-1 than in Col-0. Red lines indicate the higher expression levels of Bcoah in coi1-1 but

lower in *npr1-1*. Blue lines indicate the highest expression levels of *Bcoah* are in Col-0. Dark
green lines indicate the higher expression levels of *Bcoah* in *npr1-1* but lower in *coi1-1*.

870 Figure 5-figure supplemental 1. Genomic location of *B. cinerea* gene co-expression

- 871 **networks.** The circle diagrams showed the genome-wide distribution of gene pairs identified by
- 872 B. cinerea gene co-expression networks (GCNs) under Arabidopsis wild-type Col-0. (A) to (J)
- 873 Genomic locations of gene pairs identified by GCNs: (A) Vesicle/virulence, (B)
- translation/growth, (C) botcinic acid (BOA), (D) exocytosis regulation, (E) cyclic peptide, (F)
- 875 copper transport, (G) botrydial (BOT), (H) peptidase (gray), (I) isopentenyl pyrophosphate (IPP),
- 876 (G) polyketide. The rings show 18 B. cinerea chromosomes on a Mb scale. Genomic locations of
- 877 co-expressed gene pairs are connected by the colored lines.

878 Figure 7-figure supplemental 1. Gene co-expression networks identified from *B. cinerea*

879 transcriptomic responses to Arabidopsis wild-type Col-0 immunity. B. cinerea gene co-

880 expression networks (GCNs) were identified from 96 B. cinerea isolates infecting on

881 Arabidopsis wild-type Col-0. The similarity matrix is computed using Spearman's rank

- correlation coefficient. All co-expressed gene pairs with correlation greater than 0.85 were
- shown. Nodes with different colors represent *B. cinerea* genes condensed in GCNs with different

biological functions. Edges represent the Spearman's rank correlation coefficients between gene

pairs. GCNs were ordered as number of nodes within each network. GCNs were named after

- their biological functions, which were determined by hub and bottleneck genes within each
- 887 network: vesicle/virulence (red), translation/growth (green), botcinic acid (BOA, blue),
- 888 exocytosis regulation (pink), cyclic peptide (yellow), copper transport (slate blue), botrydial
- 889 (BOT, purple), peptidase (gray), isopentenyl pyrophosphate (IPP, turquoise), polyketide (violet).

890 Figure 7-figure supplemental 2. Gene co-expression networks identified from B. cinerea 891 transcriptomic responses to Arabidopsis jasmonate-compromised immunity. B. cinerea 892 gene co-expression networks (GCNs) were identified from 96 B. cinerea isolates infecting on 893 Arabidopsis jasmonate insensitive mutant *coil-1*. The similarity matrix is computed using 894 Spearman's rank correlation coefficient. All co-expressed gene pairs with correlation greater 895 than 0.8 were shown. Nodes with different colors represent *B. cinerea* genes condensed in GCNs 896 with different biological functions. Nodes were marked with same color as under Arabidopsis 897 wild-type Col-0 background. Nodes specifically condenced in GCNs under Arabidopsis mutant 898 *coil-1* background are marked with orange color. Edges represent the Spearman's rank 899 correlation coefficients between gene pairs. GCNs were ordered as number of nodes within each 900 network. GCNs were named after their biological functions, which were determined by hub and 901 bottleneck genes within each network: vesicle/virulence (red/orange), translation/growth 902 (green/orange), botrydial/ isopentenyl pyrophosphate (BOT/IPP, blue/turquoise/orange), botcinic 903 acid (BOA, blue), exocytosis regulation (pink), peptidase (gray/orange), copper transport (slate 904 blue/orange), plant cell wall degradation (orange), cyclic peptide (yellow), peptidase II 905 (red/orange), siderophores (orange), 26S proteasome regulated protein degradation (red/orange), 906 sugar, ROS/NO stress (orange), ATP (orange), polyketide (violet/orange).

Figure 7-figure supplemental 3. Gene co-expression networks identified from *B. cinerea*transcriptomic responses to Arabidopsis salicylic acid-compromised immunity. *B. cinerea*gene co-expression networks (GCNs) were identified from 96 *B. cinerea* isolates infecting on
Arabidopsis salicylic acid insensitive mutant *npr1-1*. The similarity matrix is computed using
Spearman's rank correlation coefficient. All co-expressed gene pairs with correlation greater
than 0.8 were shown. Nodes with different colors represent *B. cinerea* genes condensed in GCNs

913 with different biological functions. Nodes were marked with same color as under Arabidopsis 914 wild-type Col-0 background. Nodes specificaly condenced in GCNs under Arabidopsis mutant 915 *npr1-1* background are marked with orange color. Edges represent the Spearman's rank 916 correlation coefficients between gene pairs. GCNs were ordered as number of nodes within each 917 network. GCNs were named after their biological functions, which were determined by hub and 918 bottleneck genes within each network: translation/growth (green/orange), vesicle/virulence 919 (red/orange), peptidase (gray/orange), polyketide (violet/orange), botrydial/isopentenyl 920 pyrophosphate (BOT/IPP, blue/turquoise/orange), botcinic acid (BOA, blue), exocytosis 921 regulation (pink), copper transport (slate blue/orange), cyclic peptide (yellow), unknown (red), 922 sugar (orange), peptidase II (red/orange).

923 Figure 7-figure supplemental 4. Plasticity in expression profiles of genes identified by *B*.

924 cinerea gene co-expression networks under varied Arabidopsis immunities. Violin plots of

925 (A) to (O) show the expression profiles of *B. cinerea* genes in response to variation of

926 Arabidopsis immunity. Genes shown are condensed in *B. cinerea* gene co-expression networks

927 (GCNs). The model-corrected means (log₂) for *B. cinerea* transcript were used for plotting. The

928 Arabidopsis genotypes, wild-type Col-0 (purple), jasmonate insensitive mutant coil-1 (green),

929 and salicylic acid mutant *npr1-1* (orange), are shown on the x axis.

930 Figure 8-figure supplemental 1. Associations between gene co-expression networks

931 identified from co- and single-transcriptome. Venn diagrams highlights: (A) the overlap of

- 932 plant (left) and pathogen (right) genes condensed in Arabidopsis-B. cinerea gene co-expression
- 933 networks (GCNs) across three Arabidopsis genotypes, (B) the overlap of plant genes in

Arabidopsis-B. cinerea GCNs and Arabidopsis GCNs across three genotypes, (C) the overlap of
pathogen genes in Arabidopsis-*B. cinerea* GCNs and *B. cinerea* GCNs across three genotypes.

936 Figure 9-figure supplemental 1. Dual networks reveal links between Arabidopsis immunity 937 and B. cinerea virulence under coil-1 and npr1-1. Dual interaction networks were constructed 938 using gene co-expression networks (GCNs) from Arabidopsis and B. cinerea co-transcriptome 939 under JA-insensitive mutant coil-1 and SA-insensitive mutant npr1-1, respectively. The first 940 eigenvectors were derived from individual GCNs and used as input to calculate Spearman's rank 941 correlation coefficiency between GCN pairs. Green dots and orange triangles (nodes) represent 942 Arabidopsis immune- and *B. cinerea* virulence-GCNs, respectively. Blue and red lines (edges) 943 represent the positive and negative Spearman's rank correlation coefficients between GCN pairs, 944 respectively. The thickness of line signifies the correlational strength.

Figure 9-figure supplemental 2. Variation of *B. cinerea* spore germination time under *in vitro* condition.

947 Supplementary File 1. Topology traits of *B. cinerea in planta* gene co-expression networks.

948 Supplementary File 2. ANOVA table of lesion area and B. cinerea pathways. A mixed linear

949 model was fitted to test lesion area and *B. cinerea* pathways responsible for botrydial (BOT),

950 botcinic acid (BOA), and cyclic peptide (CycPep) produced under three Arabidopsis genotypes.

951 The lesion area data used in the model were GLM corrected least square means induced by 96 *B*.

952 *cinerea* isolates. Model-corrected means of transcripts from 96 *B. cinerea* isolates were z-scaled

and used in ANOVA. Df is the degrees of freedom for a term within the model. SS is the Sum of

954 Squares variation. MS is the Mean of Squared variation. F value is derived from the F statistic

and *P*-value indicates the statistical significance for a given term within the model. Significance of differences are shown as P < 0.001 '***', 0.01'**' and 0.05 '*'.

957 Supplementary File 3. ANOVA tables of *B. cinerea* gene co-expression networks. Mixed 958 linear models were fitted to individual B. cinerea (Bc) gene co-expression networks (GCNs) and 959 variation of host genotypes and Arabidopsis (At) GCNs. Variation was estimated among host 960 genotypes and first eigenvectors from four individual Arabidopsis GCNs. Df is the degrees of 961 freedom for a term within the model. SS is the Sum of Squares variation. MS is the Mean of 962 Squared variation. F value is derived from the F statistic and P-value indicates the statistical 963 significance for a given term within the model. Significance of difference are shown as P < 0.001"***", 0.01"**" and 0.05 "*". 964

965 Supplementary File 4. ANOVA tables of Arabidopsis gene co-expression networks. Linear 966 mixed models were fitted to individual Arabidopsis (At) gene co-expression networks (GCNs) 967 and variation of host genotypes and ten B. cinerea (Bc) GCNs. Variation was estimated among 968 host genotypes and first eigenvectors from individual B. cinerea GCNs. Df is the degrees of 969 freedom for a term within the model. SS is the Sum of Squares variation. MS is the Mean of 970 Squared variation. F value is derived from the F statistic and P-value indicates the statistical 971 significance for a given term within the model. Significance of difference are shown as P < 0.001"***", 0.01"**" and 0.05 "*". 972

973 Supplementary File 5. Topology traits of cross-kingdom Arabidopsis-B. cinerea gene co-

974 expression networks. Three Arabidopsis genotypes are wild-type Col-0, jasmonate insensitive

975 mutant *coil-1*, and salicylic acid insensitive mutant *npr1-1*.

976 Supplementary File 6. Analysis of potential impact of germination variation. To test if 977 germination may influence the observed network to lesion connections, we estimated 978 germination using the first principal component of genes linked to germination in Leroch et al., 979 2013. We then estimated the value of this principal component in the isolates grown on the three 980 host genotypes and conducted a linear model to compare how this eigengene links to virulence. 981 Using a linear model with and without this germination eigengene, we compared the link of the 982 10 B. cinerea transcript networks to lesion size with and without the germination eigengene 983 vector in the model.

Figure 1-source data 1. Model-corrected means of estimated *B. cinerea* biomass. *B. cinerea*biomass of 96 isolates infection on Arabidopsis genotypes was estimated using the fraction of
uniquely mapped reads against B05.10 reference genome. Three Arabidopsis genotypes are wildtype Col-0, jasmonate insensitive mutant *coi1-1*, and salicylic acid insensitive mutant *npr1-1*.

Figure 2-source data 1. Model-corrected means of *B. cinerea* transcripts. A table of modelcorrected least-square means of *B. cinerea* transcripts from 96 isolates infection on Arabidopsis
wild-type Col-0, jasmonate insensitive mutant *coi1-1*, and salicylic acid insensitive mutant *npr1- 1*.

Figure 2-source data 2. Standard errors of *B. cinerea* transcripts. A table of model-corrected
standard errors of *B. cinerea* transcripts infection on Arabidopsis wild-type Col-0, jasmonate
insensitive mutant *coil-1*, and salicylic acid insensitive mutant *npr1-1*.

Figure 2-source data 3. GLM deviance tables and broad-sense heritability of *B. cinerea*

996 transcripts. Summary of deviance tables derived from generalized linear model and estimated

997 broad-sense heritability (H^2) for *B. cinerea* transcripts. All significance values are corrected by 998 false discovery rate.

999 Figure 2-source data 4. Top 100 heritability of *B. cinerea* transcripts. Broad-sense

- 1000 heritability (H^2) of individual *B. cinerea* transcript contributed by pathogen, host and their
- 1001 interaction were estimated. Three Arabidopsis genotypes are wild-type Col-0, jasmonate
- 1002 insensitive mutant *coi1-1*, and salicylic acid insensitive mutant *npr1-1*.

1003 Figure 3-source data 1. Spearman's rank correlation between lesion area and *B. cinerea*

- 1004 transcripts abundance. A table of spearman's rank correlation coefficiency between lesion area
- 1005 and *B. cinerea* transcripts accumulation across three Arabidopsis genotypes or under individual
- 1006 genotypes. Three Arabidopsis genotypes are wild-type Col-0, jasmonate insensitive mutant coil-
- 1007 *1*, and salicylic acid insensitive mutant *npr1-1*.

1008 Figure 5-source data 1. Gene list of *B. cinerea* gene co-expression networks. Tables of *B.*

- 1009 *cinerea* genes identified by *B. cinerea* gene co-expression networks (GCNs) during 96 isolates
- 1010 infection on Arabidopsis wild-type Col-0, jasmonate insensitive mutant *coi1-1*, and salicylic acid
- 1011 insensitive mutant *npr1-1*.

1012 Figure 8-source data 1. Gene list of cross-kingdom Arabidopsis-B. cinerea gene co-

- 1013 expression networks. Tables of Arabidopsis and *B. cinerea* genes identified by co-transcriptome
- 1014 gene co-expression networks (GCNs) during 96 isolates infection on Arabidopsis wild-type Col-
- 1015 0, jasmonate insensitive mutant *coi1-1*, and salicylic acid insensitive mutant *npr1-1*.

1016 **References**

- 1017 Arbelet, D., Malfatti, P., Simond-Cote, E., Fontaine, T., Desquilbet, L., Expert, D., Kunz,
- 1018 C., and Soulie, M.C. (2010). Disruption of the Bcchs3a chitin synthase gene in Botrytis cinerea
- 1019 is responsible for altered adhesion and overstimulation of host plant immunity. Mol. Plant
- 1020 Microbe Interact. 23, 1324-1334, doi/10.1094/MPMI-02-10-0046.
- 1021 Ascari, J., Boaventura, M.A., Takahashi, J.A., Duran-Patron, R., Hernandez-Galan, R.,
- 1022 Macias-Sanchez, A.J., and Collado, I.G. (2013). Phytotoxic activity and metabolism of
- 1023 Botrytis cinerea and structure-activity relationships of isocaryolane derivatives. J. Nat. Prod. 76,
- 1024 1016-1024, doi/10.1021/np3009013.
- 1025 Atwell, S., Corwin, J.A., Soltis, N.E., Subedy, A., Denby, K.J., and Kliebenstein, D.J.
- 1026 (2015). Whole genome resequencing of Botrytis cinerea isolates identifies high levels of
- 1027 standing diversity. Front. Microbiol. **6**, 996, doi/10.3389/fmicb.2015.00996.
- 1028 Bednarek, P., Pislewska-Bednarek, M., Svatos, A., Schneider, B., Doubsky, J., Mansurova,
- 1029 M., Humphry, M., Consonni, C., Panstruga, R., Sanchez-Vallet, A., Molina, A., and
- 1030 Schulze-Lefert, P. (2009). A glucosinolate metabolism pathway in living plant cells mediates
- 1031 broad-spectrum antifungal defense. Science **323**, 101-106, doi/10.1126/science.1163732.
- 1032 Benjamini Yoav and Yekutieli Daniel (2001). The Control of the False Discovery Rate in
- 1033 Multiple Testing under Dependency. **29**, 1165-1188, doi/10.1214/aos/1013699998.
- 1034 Benton, M.J. (2009). The Red Queen and the Court Jester: species diversity and the role of
- 1035 biotic and abiotic factors through time. Science **323**, 728-732, doi/10.1126/science.1157719.

- 1036 Bergelson, J., Kreitman, M., Stahl, E.A., and Tian, D. (2001). Evolutionary dynamics of plant
- 1037 R-genes. Science **292**, 2281-2285, doi/10.1126/science.1061337.

1038 Blanco-Ulate, B., Morales-Cruz, A., Amrine, K.C., Labavitch, J.M., Powell, A.L., and

- 1039 Cantu, D. (2014). Genome-wide transcriptional profiling of Botrytis cinerea genes targeting
- 1040 plant cell walls during infections of different hosts. Front. Plant. Sci. 5, 435,
- 1041 doi/10.3389/fpls.2014.00435.

1042 Brooks, D.M., Bender, C.L., and Kunkel, B.N. (2005). The Pseudomonas syringae phytotoxin

- 1043 coronatine promotes virulence by overcoming salicylic acid-dependent defences in Arabidopsis
- 1044 thaliana. Mol. Plant. Pathol. **6**, 629-639, doi/10.1111/j.1364-3703.2005.00311.x.
- 1045 Bullard, J.H., Purdom, E., Hansen, K.D., and Dudoit, S. (2010). Evaluation of statistical
- 1046 methods for normalization and differential expression in mRNA-Seq experiments. BMC
- 1047 Bioinformatics **11**, 94, doi/10.1186/1471-2105-11-94.
- 1048 Buttner, D. and He, S.Y. (2009). Type III protein secretion in plant pathogenic bacteria. Plant
- 1049 Physiol. **150**, 1656-1664, doi/10.1104/pp.109.139089.

1050 Cantarel, B.L., Coutinho, P.M., Rancurel, C., Bernard, T., Lombard, V., and Henrissat, B.

- 1051 (2009). The Carbohydrate-Active EnZymes database (CAZy): an expert resource for
- 1052 Glycogenomics. **37**, D233–D238, doi/10.1093/nar/gkn663.
- 1053 Cao, H., Glazebrook, J., Clarke, J.D., Volko, S., and Dong, X. (1997). The Arabidopsis NPR1
- 1054 gene that controls systemic acquired resistance encodes a novel protein containing ankyrin
- 1055 repeats. Cell **88**, 57-63, doi/10.1016/S0092-8674(00)81858-9.

1056 Choquer, M., Fournier, E., Kunz, C., Levis, C., Pradier, J.M., Simon, A., and Viaud, M.

- 1057 (2007). Botrytis cinerea virulence factors: new insights into a necrotrophic and polyphageous
- 1058 pathogen. FEMS Microbiol. Lett. **277**, 1-10, doi/10.1111/j.1574-6968.2007.00930.x.
- 1059 Clay, N.K., Adio, A.M., Denoux, C., Jander, G., and Ausubel, F.M. (2009). Glucosinolate
- 1060 metabolites required for an Arabidopsis innate immune response. Science **323**, 95-101,
- 1061 doi/10.1126/science.1164627.

1062 Colmenares, A.J., Aleu, J., Duran-Patron, R., Collado, I.G., and Hernandez-Galan, R.

- 1063 (2002). The putative role of botrydial and related metabolites in the infection mechanism of
- 1064 Botrytis cinerea. J. Chem. Ecol. 28, 997-1005, doi/1015209817830.
- 1065 Colombo, M., Raposo, G., and Thery, C. (2014). Biogenesis, secretion, and intercellular
- 1066 interactions of exosomes and other extracellular vesicles. Annu. Rev. Cell Dev. Biol. 30, 255-
- 1067 289, doi/10.1146/annurev-cellbio-101512-122326.
- 1068 Conesa, A., Gotz, S., Garcia-Gomez, J.M., Terol, J., Talon, M., and Robles, M. (2005).
- 1069 Blast2GO: a universal tool for annotation, visualization and analysis in functional genomics
- 1070 research. Bioinformatics **21**, 3674-3676, doi/10.1093/bioinformatics/bti610.

1071 Corwin, J.A., Copeland, D., Feusier, J., Subedy, A., Eshbaugh, R., Palmer, C., Maloof, J.,

- 1072 and Kliebenstein, D.J. (2016). The Quantitative Basis of the Arabidopsis Innate Immune
- 1073 System to Endemic Pathogens Depends on Pathogen Genetics. PLoS Genet. 12, e1005789,
- 1074 doi/10.1371/journal.pgen.1005789.

- 1075 Corwin, J.A., Subedy, A., Eshbaugh, R., and Kliebenstein, D.J. (2016). Expansive
- 1076 Phenotypic Landscape of Botrytis cinerea Shows Differential Contribution of Genetic Diversity
- 1077 and Plasticity. Mol. Plant Microbe Interact. 29, 287-298, doi/10.1094/MPMI-09-15-0196-R.
- 1078 Corwin, J.A. and Kliebenstein, D.J. (2017). Quantitative Resistance: More Than Just
- 1079 Perception of a Pathogen. Plant Cell **29**, 655-665, doi/10.1105/tpc.16.00915.
- 1080 Courtade, G., Wimmer, R., Røhr, ÅK., Preims, M., Felice, A.K.G., Dimarogona, M., Vaaje-
- 1081 Kolstad, G., Sørlie, M., Sandgren, M., Ludwig, R., Eijsink, V.G.H., and Aachmann, F.L.
- 1082 (2016). Interactions of a fungal lytic polysaccharide monooxygenase with β -glucan substrates
- 1083 and cellobiose dehydrogenase. **113**, 5922, doi/10.1073/pnas.1602566113.
- 1084 **Couto, D. and Zipfel, C.** (2016). Regulation of pattern recognition receptor signalling in plants.
- 1085 Nat. Rev. Immunol. 16, 537-552, doi/10.1038/nri.2016.77.
- 1086 Cui, H., Qiu, J., Zhou, Y., Bhandari, D.D., Zhao, C., Bautor, J., and Parker, J.E. (2018).
- 1087 Antagonism of Transcription Factor MYC2 by EDS1/PAD4 Complexes Bolsters Salicylic Acid
- 1088 Defense in Arabidopsis Effector-Triggered Immunity. Mol. Plant. 11, 1053-1066,
- 1089 doi/10.1016/j.molp.2018.05.007.
- 1090 Dalmais, B., Schumacher, J., Moraga, J., LE Pêcheur, P., Tudzynski, B., Collado, I.G., and
- 1091 Viaud, M. (2011). The Botrytis cinerea phytotoxin botcinic acid requires two polyketide
- 1092 synthases for production and has a redundant role in virulence with botrydial. 12, 564,
- 1093 doi/10.1111/j.1364-3703.2010.00692.x.

1094 Dangl, J.L. and Jones, J.D. (2001). Plant pathogens and integrated defence responses to

- 1095 infection. Nature **411**, 826-833, doi/10.1038/35081161.
- 1096 Deighton, N., Muckenschnabel, I., Colmenares, A.J., Collado, I.G., and Williamson, B.
- 1097 (2001). Botrydial is produced in plant tissues infected by Botrytis cinerea. Phytochemistry **57**,
- 1098 689-692, doi/10.1016/S0031-9422(01)00088-7.
- 1099 Denby, K.J., Kumar, P., and Kliebenstein, D.J. (2004). Identification of Botrytis cinerea
- susceptibility loci in Arabidopsis thaliana. Plant J. 38, 473-486, doi/10.1111/j.0960-
- 1101 7412.2004.02059.x.
- 1102 **Ding Qiong and Zhang Jinlong** (2012). seqRFLP: Simulation and visualization of restriction
- 1103 enzyme cutting pattern from DNA sequences. **R package version 1.0.1.,** .
- 1104 Fordyce, R.F., Soltis, N.E., Caseys, C., Gwinner, R., Corwin, J.A., Atwell, S., Copeland, D.,
- 1105 Feusier, J., Subedy, A., Eshbaugh, R., and Kliebenstein, D.J. (2018). Digital Imaging
- 1106 Combined with Genome-Wide Association Mapping Links Loci to Plant-Pathogen Interaction
- 1107 Traits. Plant Physiol., doi/10.1104/pp.18.00851.
- 1108 Fox, J. and Weisberg, S. (2011). An R Companion to Applied Regression, Second Edition ed.
- 1109 (Sage, CA: Thousand Oaks).
- 1110 Frerigmann, H., Pislewska-Bednarek, M., Sanchez-Vallet, A., Molina, A., Glawischnig, E.,
- 1111 Gigolashvili, T., and Bednarek, P. (2016). Regulation of Pathogen-Triggered Tryptophan
- 1112 Metabolism in Arabidopsis thaliana by MYB Transcription Factors and Indole Glucosinolate
- 1113 Conversion Products. Mol. Plant. 9, 682-695, doi/10.1016/j.molp.2016.01.006.

1114	Gerbi, C., Bata, J., Breton, A., and Prensier, G. (1996). Glycoside and polysaccharide
1115	hydrolase activity of the rumen anaerobic fungus Caecomyces communis (Sphaeromonas
1116	communis SENSU ORPIN) at early and final stages of the developmental cycle. Curr. Microbiol.
1117	32, 256-259, doi/10.1007/s002849900046.

Glazebrook, J. (2005). Contrasting mechanisms of defense against biotrophic and necrotrophic

- 1119 pathogens. Annu. Rev. Phytopathol. 43, 205-227, doi/10.1146/annurev.phyto.43.040204.135923.
- 1120 Gotz, S., Garcia-Gomez, J.M., Terol, J., Williams, T.D., Nagaraj, S.H., Nueda, M.J.,

1121 Robles, M., Talon, M., Dopazo, J., and Conesa, A. (2008). High-throughput functional

- annotation and data mining with the Blast2GO suite. Nucleic Acids Res. **36**, 3420-3435,
- 1123 doi/10.1093/nar/gkn176.

1118

Govrin, E.M. and Levine, A. (2000). The hypersensitive response facilitates plant infection by
the necrotrophic pathogen Botrytis cinerea. Curr. Biol. 10, 751-757, doi/10.1016/S0960-

1126 9822(00)00560-1.

- 1127 Greenberg, J.T., Guo, A., Klessig, D.F., and Ausubel, F.M. (1994). Programmed cell death in
- 1128 plants: a pathogen-triggered response activated coordinately with multiple defense functions.

1129 Cell **77**, 551-563, doi/10.1016/0092-8674(94)90217-8.

- 1130 Igarashi, K., Uchihashi, T., Uchiyama, T., Sugimoto, H., Wada, M., Suzuki, K., Sakuda, S.,
- 1131 Ando, T., Watanabe, T., and Samejima, M. (2014). Two-way traffic of glycoside hydrolase
- 1132 family 18 processive chitinases on crystalline chitin. Nat. Commun. 5, 3975,
- 1133 doi/10.1038/ncomms4975.

- 1134 Ingo Morgenstern, Justin Powlowski, and Adrian Tsang (2014). Fungal cellulose degradation
- 1135 by oxidative enzymes: from dysfunctional GH61 family to powerful lytic polysaccharide
- 1136 monooxygenase family. **13**, 471, doi/10.1093/bfgp/elu032.
- 1137 Jones, J.D. and Dangl, J.L. (2006). The plant immune system. Nature 444, 323-329,
- 1138 doi/10.1038/nature05286.

1139 Kanzaki, H., Yoshida, K., Saitoh, H., Fujisaki, K., Hirabuchi, A., Alaux, L., Fournier, E.,

- 1140 Tharreau, D., and Terauchi, R. (2012). Arms race co-evolution of Magnaporthe oryzae AVR-
- 1141 Pik and rice Pik genes driven by their physical interactions. Plant J. 72, 894-907,
- 1142 doi/10.1111/j.1365-313X.2012.05110.x.
- 1143 Karasov, T.L., Kniskern, J.M., Gao, L., DeYoung, B.J., Ding, J., Dubiella, U., Lastra, R.O.,

1144 Nallu, S., Roux, F., Innes, R.W., Barrett, L.G., Hudson, R.R., and Bergelson, J. (2014). The

1145 long-term maintenance of a resistance polymorphism through diffuse interactions. Nature **512**,

- 1146 436-440, doi/10.1038/nature13439.
- 1147 Kliebenstein, D.J., Rowe, H.C., and Denby, K.J. (2005). Secondary metabolites influence

1148 Arabidopsis/Botrytis interactions: variation in host production and pathogen sensitivity. Plant J.

1149 **44,** 25-36, doi/10.1111/j.1365-313X.2005.02508.x.

- 1150 Krishnakumar, V., Hanlon, M.R., Contrino, S., Ferlanti, E.S., Karamycheva, S., Kim, M.,
- 1151 Rosen, B.D., Cheng, C.Y., Moreira, W., Mock, S.A., Stubbs, J., Sullivan, J.M., Krampis, K.,
- 1152 Miller, J.R., Micklem, G., Vaughn, M., and Town, C.D. (2015). Araport: the Arabidopsis
- 1153 information portal. Nucleic Acids Res. 43, 1003, doi/10.1093/nar/gku1200.

- 1154 Kubicek, C.P., Starr, T.L., and Glass, N.L. (2014). Plant cell wall-degrading enzymes and
- their secretion in plant-pathogenic fungi. Annu. Rev. Phytopathol. 52, 427-451,
- 1156 doi/10.1146/annurev-phyto-102313-045831.
- 1157 Kumar, R., Ichihashi, Y., Kimura, S., Chitwood, D.H., Headland, L.R., Peng, J., Maloof,
- 1158 J.N., and Sinha, N.R. (2012). A High-Throughput Method for Illumina RNA-Seq Library
- 1159 Preparation. Front. Plant. Sci. **3**, 202, doi/10.3389/fpls.2012.00202.
- 1160 Lamesch, P., Dreher, K., Swarbreck, D., Sasidharan, R., Reiser, L., and Huala, E. (2010).
- 1161 Using the Arabidopsis information resource (TAIR) to find information about Arabidopsis genes.
- 1162 Curr. Protoc. Bioinformatics Chapter 1, Unit1.11, doi/10.1002/cpbi.36.
- 1163 Lamesch, P., Berardini, T.Z., Li, D., Swarbreck, D., Wilks, C., Sasidharan, R., Muller, R.,
- 1164 Dreher, K., Alexander, D.L., Garcia-Hernandez, M., Karthikeyan, A.S., Lee, C.H., Nelson,
- 1165 W.D., Ploetz, L., Singh, S., Wensel, A., and Huala, E. (2012). The Arabidopsis Information
- 1166 Resource (TAIR): improved gene annotation and new tools. Nucleic Acids Res. 40, 1202,
- 1167 doi/10.1093/nar/gkr1090.
- 1168 Langfelder, P. and Horvath, S. (2008). WGCNA: an R package for weighted correlation
- 1169 network analysis. BMC Bioinformatics **9**, 559, doi/10.1186/1471-2105-9-559.
- 1170 Langmead, B., Trapnell, C., Pop, M., and Salzberg, S.L. (2009). Ultrafast and memory-
- 1171 efficient alignment of short DNA sequences to the human genome. Genome Biol. 10, r25. Epub
- 1172 2009 Mar 4, doi/10.1186/gb-2009-10-3-r25.

- 1173 Lanver, D., Muller, A.N., Happel, P., Schweizer, G., Haas, F.B., Franitza, M., Pellegrin, C.,
- 1174 Reissmann, S., Altmuller, J., Rensing, S.A., and Kahmann, R. (2018). The Biotrophic
- 1175 Development of Ustilago maydis Studied by RNA-Seq Analysis. Plant Cell **30**, 300-323,
- 1176 doi/10.1105/tpc.17.00764.
- 1177 Lee, H.J., Georgiadou, A., Walther, M., Nwakanma, D., Stewart, L.B., Levin, M., Otto,
- 1178 **T.D., Conway, D.J., Coin, L.J., and Cunnington, A.J.** (2018). Integrated pathogen load and
- 1179 dual transcriptome analysis of systemic host-pathogen interactions in severe malaria. Sci. Transl.
- 1180 Med. **10**, 10.1126/scitranslmed.aar3619, doi/10.1126/scitranslmed.aar3619.
- 1181 Leroch, M., Kleber, A., Silva, E., Coenen, T., Koppenhofer, D., Shmaryahu, A., Valenzuela,
- 1182 **P.D., and Hahn, M.** (2013). Transcriptome profiling of Botrytis cinerea conidial germination
- 1183 reveals upregulation of infection-related genes during the prepenetration stage. Eukaryot. Cell.
- 1184 **12,** 614-626, doi/10.1128/EC.00295-12 [doi].
- 1185 Li, H., Handsaker, B., Wysoker, A., Fennell, T., Ruan, J., Homer, N., Marth, G., Abecasis,
- 1186 G., Durbin, R., and 1000 Genome Project Data Processing Subgroup (2009). The Sequence
- 1187 Alignment/Map format and SAMtools. Bioinformatics **25**, 2078-2079,
- 1188 doi/10.1093/bioinformatics/btp352.
- 1189 Macheleidt, J., Mattern, D.J., Fischer, J., Netzker, T., Weber, J., Schroeckh, V., Valiante,
- 1190 V., and Brakhage, A.A. (2016). Regulation and Role of Fungal Secondary Metabolites. Annu.
- 1191 Rev. Genet. **50**, 371-392, doi/10.1146/annurev-genet-120215-035203.

- 1192 McClure, R.S., Overall, C.C., Hill, E.A., Song, H.S., Charania, M., Bernstein, H.C.,
- 1193 McDermott, J.E., and Beliaev, A.S. (2018). Species-specific transcriptomic network inference
- 1194 of interspecies interactions. ISME J. 12, 2011-2023, doi/10.1038/s41396-018-0145-6.
- 1195 Mengiste, T., Chen, X., Salmeron, J., and Dietrich, R. (2003). The BOTRYTIS
- 1196 SUSCEPTIBLE1 gene encodes an R2R3MYB transcription factor protein that is required for
- 1197 biotic and abiotic stress responses in Arabidopsis. Plant Cell 15, 2551-2565,
- 1198 doi/10.1105/tpc.014167.
- 1199 Mengiste, T. (2012). Plant immunity to necrotrophs. Annu. Rev. Phytopathol. 50, 267-294,
- 1200 doi/10.1146/annurev-phyto-081211-172955.
- Mine, A., Seyfferth, C., Kracher, B., Berens, M.L., Becker, D., and Tsuda, K. (2018). The
 Defense Phytohormone Signaling Network Enables Rapid, High-Amplitude Transcriptional
 Reprogramming during Effector-Triggered Immunity. Plant Cell 30, 1199-1219,

1204 doi/10.1105/tpc.17.00970.

- Mittal, S. and Davis, K.R. (1995). Role of the phytotoxin coronatine in the infection of
 Arabidopsis thaliana by Pseudomonas syringae pv. tomato. Mol. Plant Microbe Interact. 8, 1651207 171.
- 1208 Moraga, J., Dalmais, B., Izquierdo-Bueno, I., Aleu, J., Hanson, J.R., Hernandez-Galan, R.,
- 1209 Viaud, M., and Collado, I.G. (2016). Genetic and Molecular Basis of Botrydial Biosynthesis:
- 1210 Connecting Cytochrome P450-Encoding Genes to Biosynthetic Intermediates. ACS Chem. Biol.
- 1211 **11**, 2838-2846, doi/10.1021/acschembio.6b00581.

- 1212 Movahedi, S., Norey, C.G., Kay, J., and Heale, J.B. (1991). Infection and pathogenesis of cash
- 1213 crops by Botrytis cinerea: primary role of an aspartic proteinase. **306**, 213.

1214 Musungu, B.M., Bhatnagar, D., Brown, R.L., Payne, G.A., OBrian, G., Fakhoury, A.M.,

- 1215 and Geisler, M. (2016). A Network Approach of Gene Co-expression in the Zea
- 1216 mays/Aspergillus flavus Pathosystem to Map Host/Pathogen Interaction Pathways. Front. Genet.
- 1217 **7**, 206, doi/10.3389/fgene.2016.00206.

1218 Nelson, C.E., Attia, M.A., Rogowski, A., Morland, C., Brumer, H., and Gardner, J.G.

- 1219 (2017). Comprehensive functional characterization of the glycoside hydrolase family 3 enzymes
- 1220 from Cellvibrio japonicus reveals unique metabolic roles in biomass saccharification. Environ.
- 1221 Microbiol. **19**, 5025-5039, doi/10.1111/1462-2920.13959.

1222 Nobori, T., Velasquez, A.C., Wu, J., Kvitko, B.H., Kremer, J.M., Wang, Y., He, S.Y., and

- 1223 **Tsuda, K.** (2018). Transcriptome landscape of a bacterial pathogen under plant immunity. Proc.
- 1224 Natl. Acad. Sci. U. S. A. 115, E3064, doi/10.1073/pnas.1800529115.

1225 Okada, H., Ebhardt, H.A., Vonesch, S.C., Aebersold, R., and Hafen, E. (2016). Proteome-

- 1226 wide association studies identify biochemical modules associated with a wing-size phenotype in
- 1227 Drosophila melanogaster. Nat. Commun. 7, 12649, doi/10.1038/ncomms12649.
- 1228 Pages, H., Aboyoun, P., Gentleman, R., and DebRoy, S. (2017). Biostrings: String objects
- 1229 representing biological sequences, and matching algorithms. **R package version 2.44.2.**, .

- 1230 Pérez-Izquierdo, L., Morin, E., Maurice, J.P., Martin, F., Rincón, A., and Buée, M. (2017).
- 1231 A new promising phylogenetic marker to study the diversity of fungal communities: The
- 1232 Glycoside Hydrolase 63 gene. **17**, e11, doi/10.1111/1755-0998.12678.
- 1233 Pieterse, C.M. and Van Loon, L.C. (2004). NPR1: the spider in the web of induced resistance
- 1234 signaling pathways. Curr. Opin. Plant Biol. 7, 456-464, doi/10.1016/j.pbi.2004.05.006.
- 1235 Pinedo, C., Wang, C., Pradier, J., Dalmais, B., Choquer, M., Le Pêcheur, P., Morgant, G.,
- 1236 Collado, I.G., Cane, D.E., and Viaud, M. (2008). Sesquiterpene synthase from the botrydial
- 1237 biosynthetic gene cluster of the phytopathogen Botrytis cinerea. **3**, 791, doi/10.1021/cb800225v.
- 1238 Porquier, A., Morgant, G., Moraga, J., Dalmais, B., Luyten, I., Simon, A., Pradier, J.M.,
- 1239 Amselem, J., Collado, I.G., and Viaud, M. (2016). The botrydial biosynthetic gene cluster of
- 1240 Botrytis cinerea displays a bipartite genomic structure and is positively regulated by the putative
- 1241 Zn(II)2Cys6 transcription factor BcBot6. Fungal Genet. Biol. 96, 33-46,
- 1242 doi/10.1016/j.fgb.2016.10.003.
- 1243 Porquier, A., Moraga, J., Morgant, G., Dalmais, B., Simon, A., Sghyer, H., Collado, I., and
- 1244 Viaud, M. (2019). Botcinic acid biosynthesis in Botrytis cinerea relies on a subtelomeric gene
- 1245 cluster surrounded by relics of transposons and is regulated by the Zn2Cys6 transcription factor
- 1246 BcBoa13(), doi/10.1007/s00294-019-00952-4.
- Poussereau, N., Creton, S., Billon-Grand, G., Rascle, C., and Fevre, M. (2001). Regulation of
 acp1, encoding a non-aspartyl acid protease expressed during pathogenesis of Sclerotinia
- 1249 sclerotiorum. Microbiology **147**, 717-726, doi/10.1099/00221287-147-3-717.

1250	Poussereau, N., Gente, S., Rascle, C., Billon-Grand, G., and Fevre, M. (2001). aspS encoding
1251	an unusual aspartyl protease from Sclerotinia sclerotiorum is expressed during
1252	phytopathogenesis. FEMS Microbiol. Lett. 194, 27-32, doi/S0378-1097(00)00500-0 [pii].
1253	R Core Team (2014). R: A Language and Environment for Statistical Computing(Vienna,
1254	Austria).

1255 **Robinson, M.D. and Smyth, G.K.** (2008). Small-sample estimation of negative binomial

1256 dispersion, with applications to SAGE data. Biostatistics 9, 321-332,

1257 doi/10.1093/biostatistics/kxm030.

Robinson, M.D. and Oshlack, A. (2010). A scaling normalization method for differential
expression analysis of RNA-seq data. Genome Biol. 11, r25. Epub 2010 Mar 2, doi/10.1186/gb2010-11-3-r25.

Rodrigues, M.L., Godinho, R.M., Zamith-Miranda, D., and Nimrichter, L. (2015). Traveling
into Outer Space: Unanswered Questions about Fungal Extracellular Vesicles. PLoS Pathog. 11,
e1005240, doi/10.1371/journal.ppat.1005240.

1264 Rossi, F.R., Garriz, A., Marina, M., Romero, F.M., Gonzalez, M.E., Collado, I.G., and

1265 **Pieckenstain, F.L.** (2011). The sesquiterpene botrydial produced by Botrytis cinerea induces the

1266 hypersensitive response on plant tissues and its action is modulated by salicylic acid and

1267 jasmonic acid signaling. Mol. Plant Microbe Interact. 24, 888-896, doi/10.1094/MPMI-10-10-

1268 0248.

- 1269 Rowe, H.C. and Kliebenstein, D.J. (2007). Elevated genetic variation within virulence-
- 1270 associated Botrytis cinerea polygalacturonase loci. Mol. Plant Microbe Interact. 20, 1126-1137,
- 1271 doi/10.1094/MPMI-20-9-1126.
- 1272 **Russell V. Lenth** (2016). Least-Squares Means: The R Package Ismeans. 69, 1-33,
- 1273 doi/10.18637/jss.v069.i01.
- 1274 Samuel, M., Bleackley, M., Anderson, M., and Mathivanan, S. (2015). Extracellular vesicles
- 1275 including exosomes in cross kingdom regulation: a viewpoint from plant-fungal interactions.
- 1276 Front. Plant. Sci. 6, 766, doi/10.3389/fpls.2015.00766.
- 1277 Schumacher, J., Pradier, J.M., Simon, A., Traeger, S., Moraga, J., Collado, I.G., Viaud, M.,
- 1278 and Tudzynski, B. (2012). Natural variation in the VELVET gene bevel1 affects virulence and
- 1279 light-dependent differentiation in Botrytis cinerea. PLoS One 7, e47840,
- 1280 doi/10.1371/journal.pone.0047840.
- 1281 Schumacher, J., Simon, A., Cohrs, K.C., Traeger, S., Porquier, A., Dalmais, B., Viaud, M.,
- 1282 and Tudzynski, B. (2015). The VELVET Complex in the Gray Mold Fungus Botrytis cinerea:
- 1283 Impact of BcLAE1 on Differentiation, Secondary Metabolism, and Virulence. Mol. Plant
- 1284 Microbe Interact. 28, 659-674, doi/10.1094/MPMI-12-14-0411-R.
- 1285 Shannon, P., Markiel, A., Ozier, O., Baliga, N.S., Wang, J.T., Ramage, D., Amin, N.,
- 1286 Schwikowski, B., and Ideker, T. (2003). Cytoscape: a software environment for integrated
- 1287 models of biomolecular interaction networks. Genome Res. 13, 2498-2504,
- 1288 doi/10.1101/gr.1239303.

1289	Sharma, H.C., Pampapathy, G., Dhillon, M.K., and Ridsdill-Smith, J.T. (2005). Detached
1290	leaf assay to screen for host plant resistance to Helicoverpa armigera. J. Econ. Entomol. 98, 568-
1291	576, doi/10.1603/0022-0493-98.2.568.

- 1292 Siewers, V., Viaud, M., Jimenez-Teja, D., Collado, I.G., Gronover, C.S., Pradier, J.,
- 1293 Tudzynski, B., and Tudzynski, P. (2005). Functional analysis of the cytochrome P450
- 1294 monooxygenase gene bcbot1 of Botrytis cinerea indicates that botrydial is a strain-specific
- 1295 virulence factor. **18**, 602, doi/10.1094/MPMI-18-0602.
- 1296 Soltis, N.E., Atwell, S., Shi, G., Fordyce, R., Gwinner, R., Gao, D., Shafi, A., and
- 1297 Kliebenstein, D. (2018). Crop domestication and pathogen virulence: Interactions of tomato and
- 1298 *Botrytis* genetic diversity., doi/10.1101/255992.
- 1299 Soltis, N.E., Zhang, W., Corwin, J.A., Atwell, S., and Kliebenstein, D.J. (2019). Pathogen
- 1300 genetic control of transcriptome variation in the Arabidopsis thaliana Botrytis cinerea
- 1301 pathosystem. 577585, doi/10.1101/577585.
- 1302 Stefanato, F.L., Abou-Mansour, E., Buchala, A., Kretschmer, M., Mosbach, A., Hahn, M.,
- 1303 Bochet, C.G., Metraux, J.P., and Schoonbeek, H.J. (2009). The ABC transporter BcatrB from
- 1304 Botrytis cinerea exports camalexin and is a virulence factor on Arabidopsis thaliana. Plant J. 58,
- 1305 499-510, doi/10.1111/j.1365-313X.2009.03794.x.
- Stergiopoulos, I. and de Wit, P.J. (2009). Fungal effector proteins. Annu. Rev. Phytopathol. 47,
 233-263, doi/10.1146/annurev.phyto.112408.132637.

- Stuart, J.M., Segal, E., Koller, D., and Kim, S.K. (2003). A gene-coexpression network for
 global discovery of conserved genetic modules. Science 302, 249-255,
- 1310 doi/10.1126/science.1087447.
- 1311 Swierzy, I.J., Handel, U., Kaever, A., Jarek, M., Scharfe, M., Schluter, D., and Luder,
- 1312 C.G.K. (2017). Divergent co-transcriptomes of different host cells infected with Toxoplasma
- gondii reveal cell type-specific host-parasite interactions. Sci. Rep. 7, w, doi/10.1038/s41598017-07838-w.
- 1315 Tang, D., Wang, G., and Zhou, J.M. (2017). Receptor Kinases in Plant-Pathogen Interactions:
- 1316 More Than Pattern Recognition. Plant Cell **29**, 618-637, doi/10.1105/tpc.16.00891.
- 1317 Tayal, P., Raj, S., Sharma, E., Kumar, M., Dayaman, V., Verma, N., Jogawat, A., Dua, M.,
- 1318 Kapoor, R., and Johri, A.K. (2017). A Botrytis cinerea KLP-7 Kinesin acts as a Virulence
- 1319 Determinant during Plant Infection. Sci. Rep. 7, 5, doi/10.1038/s41598-017-09409-5.
- 1320 ten Have, A., Dekkers, E., Kay, J., Phylip, L.H., and van Kan, J.A. (2004). An aspartic
- 1321 proteinase gene family in the filamentous fungus Botrytis cinerea contains members with novel
- 1322 features. Microbiology **150**, 2475-2489, doi/10.1099/mic.0.27058-0.
- 1323 ten Have, A., Espino, J.J., Dekkers, E., Van Sluyter, S.C., Brito, N., Kay, J., Gonzalez, C.,
- 1324 and van Kan, J.A. (2010). The Botrytis cinerea aspartic proteinase family. Fungal Genet. Biol.
- 1325 **47**, 53-65, doi/10.1016/j.fgb.2009.10.008.
- 1326 Tien-chye Tan, Daniel Kracher, Rosaria Gandini, Christoph Sygmund, Roman Kittl,
- 1327 Dietmar Haltrich, B Martin Hällberg, Roland Ludwig, and Christina Divne (2015).

- 1328 Structural basis for cellobiose dehydrogenase action during oxidative cellulose degradation. **6**,
- 1329 7542, doi/10.1038/ncomms8542.
- 1330 Toruno, T.Y., Stergiopoulos, I., and Coaker, G. (2016). Plant-Pathogen Effectors: Cellular
- 1331 Probes Interfering with Plant Defenses in Spatial and Temporal Manners. Annu. Rev.
- 1332 Phytopathol. 54, 419-441, doi/10.1146/annurev-phyto-080615-100204.
- 1333 Tsuda, K. and Katagiri, F. (2010). Comparing signaling mechanisms engaged in pattern-
- triggered and effector-triggered immunity. Curr. Opin. Plant Biol. 13, 459-465,
- 1335 doi/10.1016/j.pbi.2010.04.006.
- 1336 Urlacher, V.B. and Girhard, M. (2012). Cytochrome P450 monooxygenases: an update on
- 1337 perspectives for synthetic application. Trends Biotechnol. **30**, 26-36,
- 1338 doi/10.1016/j.tibtech.2011.06.012.
- 1339 Van Kan, J.A., Stassen, J.H., Mosbach, A., Van Der Lee, T A, Faino, L., Farmer, A.D.,
- 1340 Papasotiriou, D.G., Zhou, S., Seidl, M.F., Cottam, E., Edel, D., Hahn, M., Schwartz, D.C.,
- 1341 Dietrich, R.A., Widdison, S., and Scalliet, G. (2017). A gapless genome sequence of the
- 1342 fungus Botrytis cinerea. Mol. Plant. Pathol. 18, 75-89, doi/10.1111/mpp.12384.
- 1343 Van Vu, B., Itoh, K., Nguyen, Q.B., Tosa, Y., and Nakayashiki, H. (2012). Cellulases
- 1344 belonging to glycoside hydrolase families 6 and 7 contribute to the virulence of Magnaporthe
- 1345 oryzae. Mol. Plant Microbe Interact. **25**, 1135-1141, doi/10.1094/MPMI-02-12-0043-R.
- 1346 Venables, W.N. and Ripley, B.D. (2002). Modern Applied Statistics with S, Fourth Edition ed.
- 1347 (New York: Springer).

1348 Walker, A.S., Gladieux, P., Decognet, V., Fermaud, M., Confais, J., Roudet, J., Bardin, M.,

1349 Bout, A., Nicot, P.C., Poncet, C., and Fournier, E. (2015). Population structure and temporal

1350 maintenance of the multihost fungal pathogen Botrytis cinerea: causes and implications for

- 1351 disease management. Environ. Microbiol. **17**, 1261-1274, doi/10.1111/1462-2920.12563.
- Walz, A., Zingen-Sell, I., Loeffler, M., and Sauer, M. (2008). Expression of an oxalate oxidase
 gene in tomato and severity of disease caused by Botrytis cinerea and Sclerotinia sclerotiorum.
 57, 453-458, doi/10.1111/j.1365-3059.2007.01815.x.
- 1355 Wang, C.M., Hopson, R., Lin, X., and Cane, D.E. (2009). Biosynthesis of the sesquiterpene
- 1356 botrydial in Botrytis cinerea. Mechanism and stereochemistry of the enzymatic formation of

1357 presilphiperfolan-8beta-ol. J. Am. Chem. Soc. **131**, 8360-8361, doi/10.1021/ja9021649.

1358 Weiberg, A., Wang, M., Lin, F.M., Zhao, H., Zhang, Z., Kaloshian, I., Huang, H.D., and

1359 Jin, H. (2013). Fungal small RNAs suppress plant immunity by hijacking host RNA interference

1360 pathways. Science **342**, 118-123, doi/10.1126/science.1239705.

Westermann, A.J., Barquist, L., and Vogel, J. (2017). Resolving host-pathogen interactions by
dual RNA-seq. PLoS Pathog. 13, e1006033, doi/10.1371/journal.ppat.1006033.

Williamson, B., Tudzynski, B., Tudzynski, P., and van Kan, J.A. (2007). Botrytis cinerea: the
cause of grey mould disease. Mol. Plant. Pathol. 8, 561-580, doi/10.1111/j.1364-

1365 3703.2007.00417.x.

- 1366 Windram, O., Madhou, P., McHattie, S., Hill, C., Hickman, R., Cooke, E., Jenkins, D.J.,
- 1367 Penfold, C.A., Baxter, L., Breeze, E., Kiddle, S.J., Rhodes, J., Atwell, S., Kliebenstein, D.J.,

- 1368 Kim, Y.S., Stegle, O., Borgwardt, K., Zhang, C., Tabrett, A., Legaie, R., Moore, J.,
- 1369 Finkenstadt, B., Wild, D.L., Mead, A., Rand, D., Beynon, J., Ott, S., Buchanan-Wollaston,
- 1370 V., and Denby, K.J. (2012). Arabidopsis defense against Botrytis cinerea: chronology and
- 1371 regulation deciphered by high-resolution temporal transcriptomic analysis. Plant Cell 24, 3530-
- 1372 3557, doi/10.1105/tpc.112.102046.
- 1373 Xie, D.X., Feys, B.F., James, S., Nieto-Rostro, M., and Turner, J.G. (1998). COI1: an
- 1374 Arabidopsis gene required for jasmonate-regulated defense and fertility. Science 280, 1091-
- 1375 1094, doi/10.1126/science.280.5366.1091.
- 1376 Xu, J., Meng, J., Meng, X., Zhao, Y., Liu, J., Sun, T., Liu, Y., Wang, Q., and Zhang, S.
- 1377 (2016). Pathogen-Responsive MPK3 and MPK6 Reprogram the Biosynthesis of Indole
- 1378 Glucosinolates and Their Derivatives in Arabidopsis Immunity. Plant Cell 28, 1144-1162,
- 1379 doi/10.1105/tpc.15.00871.
- 1380 Xu, L., Liu, F., Lechner, E., Genschik, P., Crosby, W.L., Ma, H., Peng, W., Huang, D., and
- 1381 Xie, D. (2002). The SCF(COI1) ubiquitin-ligase complexes are required for jasmonate response
 1382 in Arabidopsis. Plant Cell 14, 1919-1935, doi/10.1105/tpc.003368.
- 1383 Zamocky, M., Ludwig, R., Peterbauer, C., Hallberg, B.M., Divne, C., Nicholls, P., and
- 1384 Haltrich, D. (2006). Cellobiose dehydrogenase--a flavocytochrome from wood-degrading,
- 1385 phytopathogenic and saprotropic fungi. Curr. Protein Pept. Sci. 7, 255-280,
- 1386 doi/10.2174/138920306777452367.

1387	Zhang, B. and Horvath, S. (2005). A general framework for weighted gene co-expression
1388	network analysis. Stat. Appl. Genet. Mol. Biol. 4, 6115.1128. Epub 2005 Aug 12,
1389	doi/10.2202/1544-6115.1128.

- 1390 Zhang, W., Kwon, S.T., Chen, F., and Kliebenstein, D.J. (2016). Isolate Dependency of
- 1391 Brassica rapa Resistance QTLs to Botrytis cinerea. Front. Plant. Sci. 7, 161,
- 1392 doi/10.3389/fpls.2016.00161.

1393 Zhang, W., Corwin, J.A., Copeland, D., Feusier, J., Eshbaugh, R., Chen, F., Atwell, S., and

- 1394 Kliebenstein, D.J. (2017). Plastic Transcriptomes Stabilize Immunity to Pathogen Diversity:
- 1395 The Jasmonic Acid and Salicylic Acid Networks within the Arabidopsis/Botrytis Pathosystem.
- 1396 Plant Cell **29**, 2727-2752, doi/10.1105/tpc.17.00348.

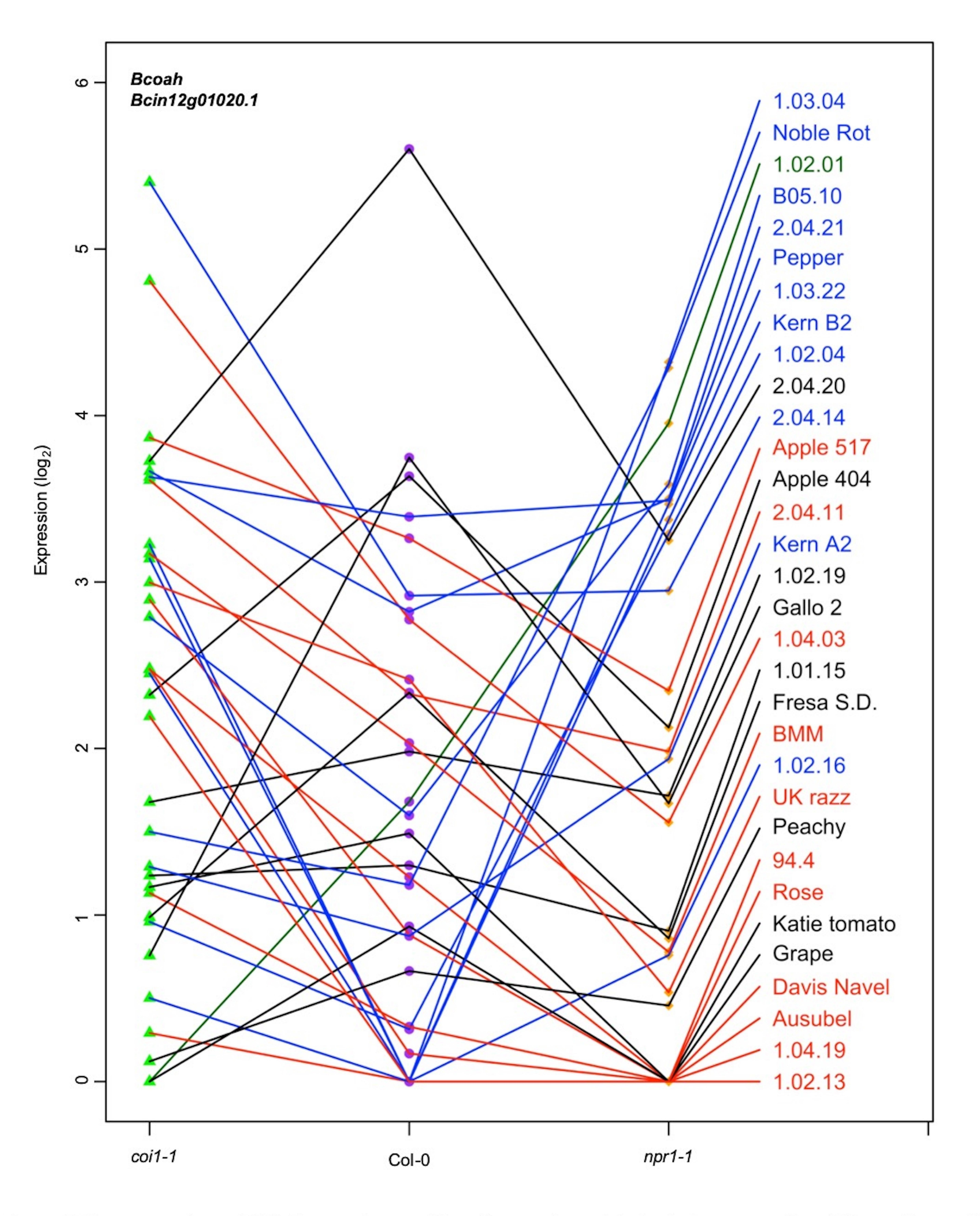
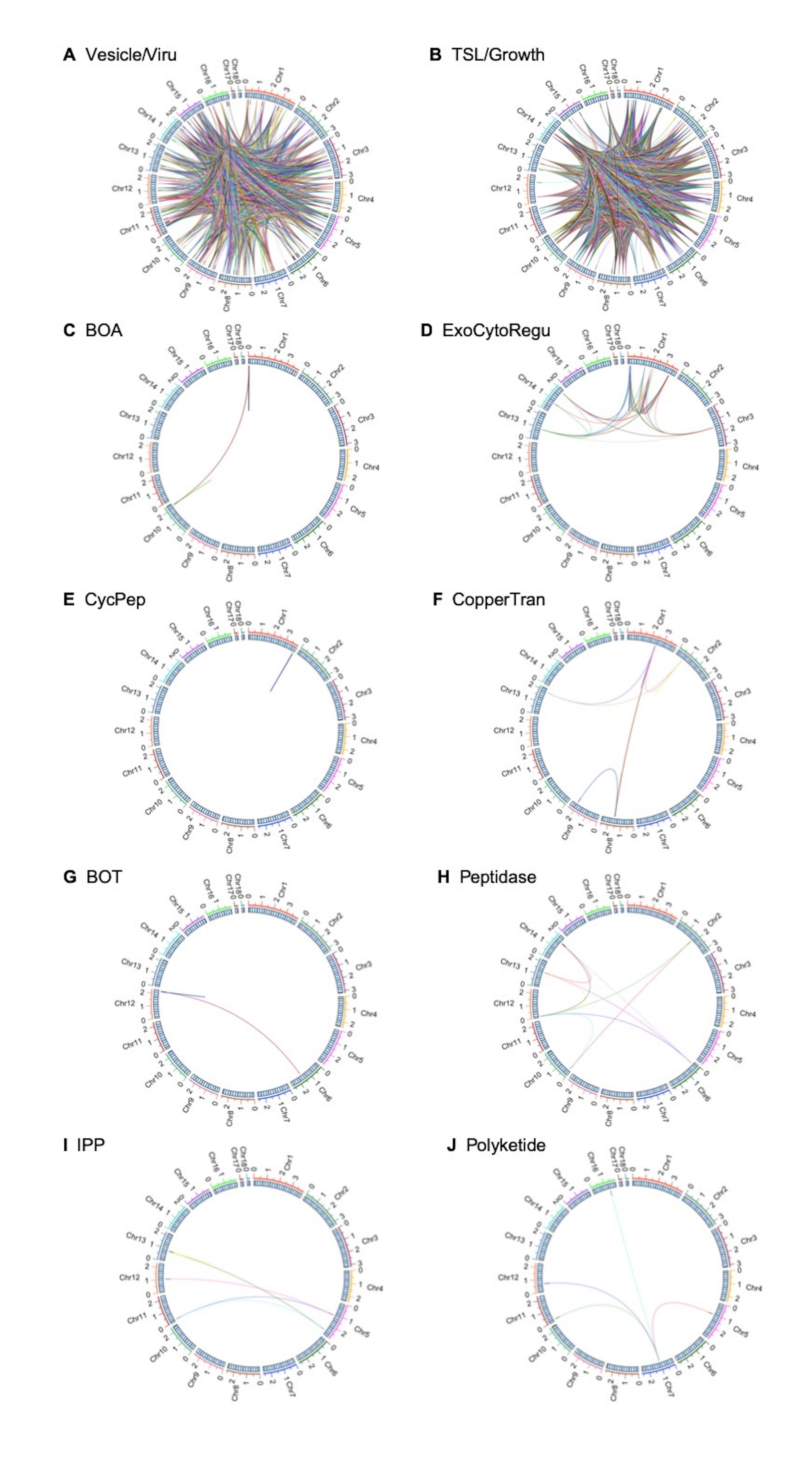
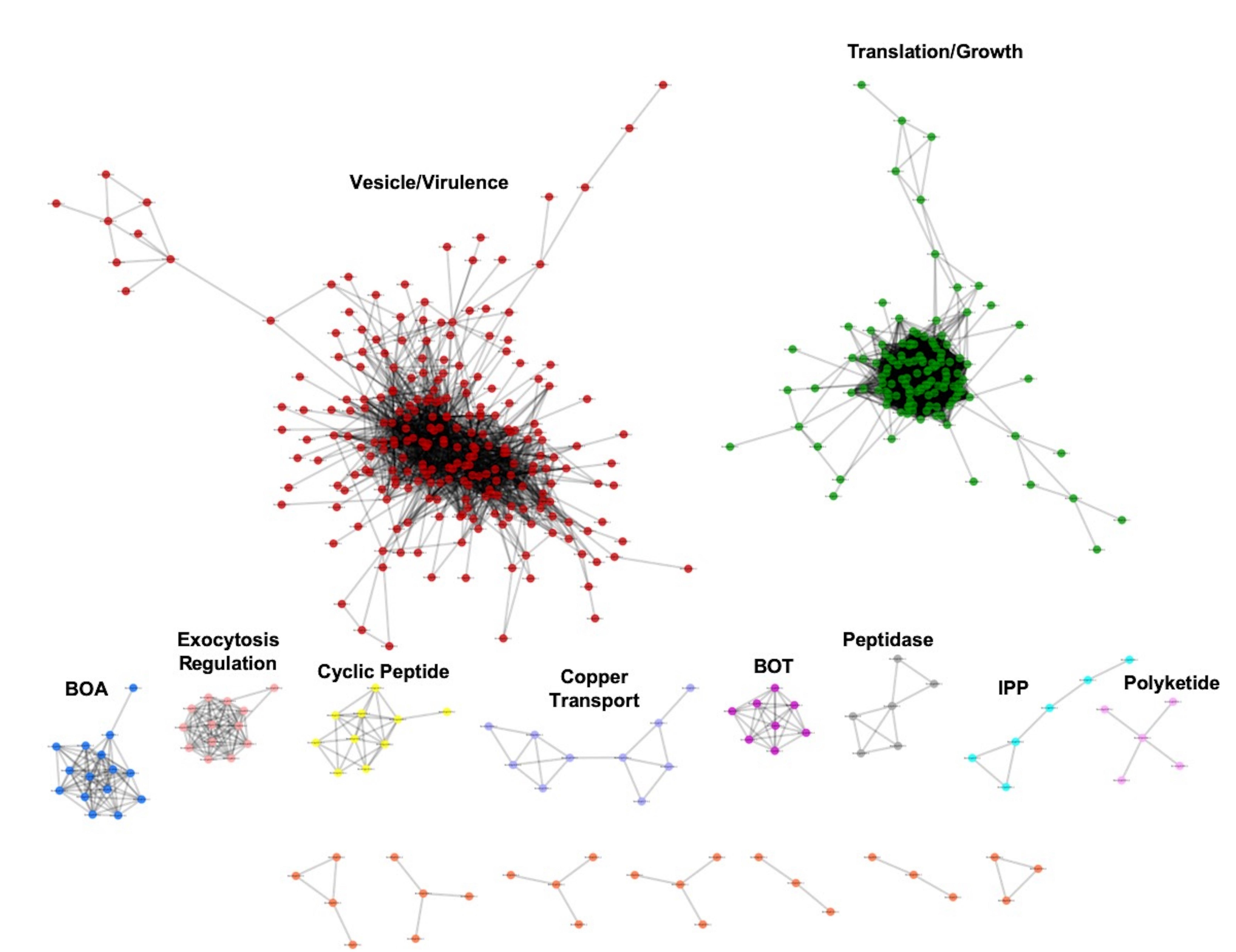


Figure 3-figure supplemental 1. Expression profiles of an oxaloacetate hydrolase gene *Bcoah* from diverse *B. cinerea* isolates across Arabidopsis genotypes. Rank plot shows the relationship o *Bcoah* expression from 32 diverse *B. cinerea* isolates (right) across three Arabidopsis genotypes (x axis). Three Arabidopsis genotypes are wild-type Col-0 (purple dot), jasmonate insensitive mutant *coi1-1* (green triangle), and salicylic acid mutant *npr1-1* (orange diamond). The model-corrected means (log₂) for the transcript of *Bcoah* (*Bcin12g01020.1*) encoding an oxaloacetate hydrolase gene are utilized for plotting. The transcript expression levels from the same isolate across three Arabidopsis genotypes are connected with a colored line. The names of 32 isolates are represented with the same colored lines as induced *Bcoah* expression levels. Black lines indicate the expression levels of *Bcoah* are higher in *coi1-1* and *npr1-1* than in Col-0. Red lines indicate the higher expression levels of *Bcoah* in *coi1-1* but lower in *npr1-1*. Blue lines indicate the highest expression levels of *Bcoah* are in Col-0. Dark green lines indicate the higher expression levels of *Bcoah* in *npr1-1* but lower in *coi1-1*.





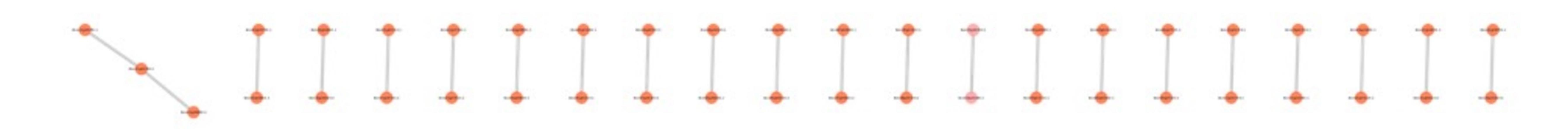


Figure 7-figure supplemental 1. Gene co-expression networks identified from *B. cinerea* transcriptomic responses to **Arabidopsis wild-type Col-0 immunity.** *B. cinerea* gene co-expression networks (GCNs) were identified from 96 *B. cinerea* isolates infecting on Arabidopsis wild-type Col-0. The similarity matrix is computed using Spearman's rank correlation coefficient. All co-expressed gene pairs with correlation greater than 0.85 were shown. Nodes with different colors represent *B. cinerea* genes condensed in GCNs with different biological functions. Edges represent the Spearman's rank correlation coefficients between gene pairs. GCNs were ordered as number of nodes within each network. GCNs were named after their biological functions, which were determined by hub and bottleneck genes within each network: vesicle/virulence (red), translation/growth (green), botcinic acid (BOA, blue), exocytosis regulation (pink), cyclic peptide (yellow), copper transport (slate blue), botrydial (BOT, purple), peptidase (gray), isopentenyl pyrophosphate (IPP, turquoise), polyketide (violet).

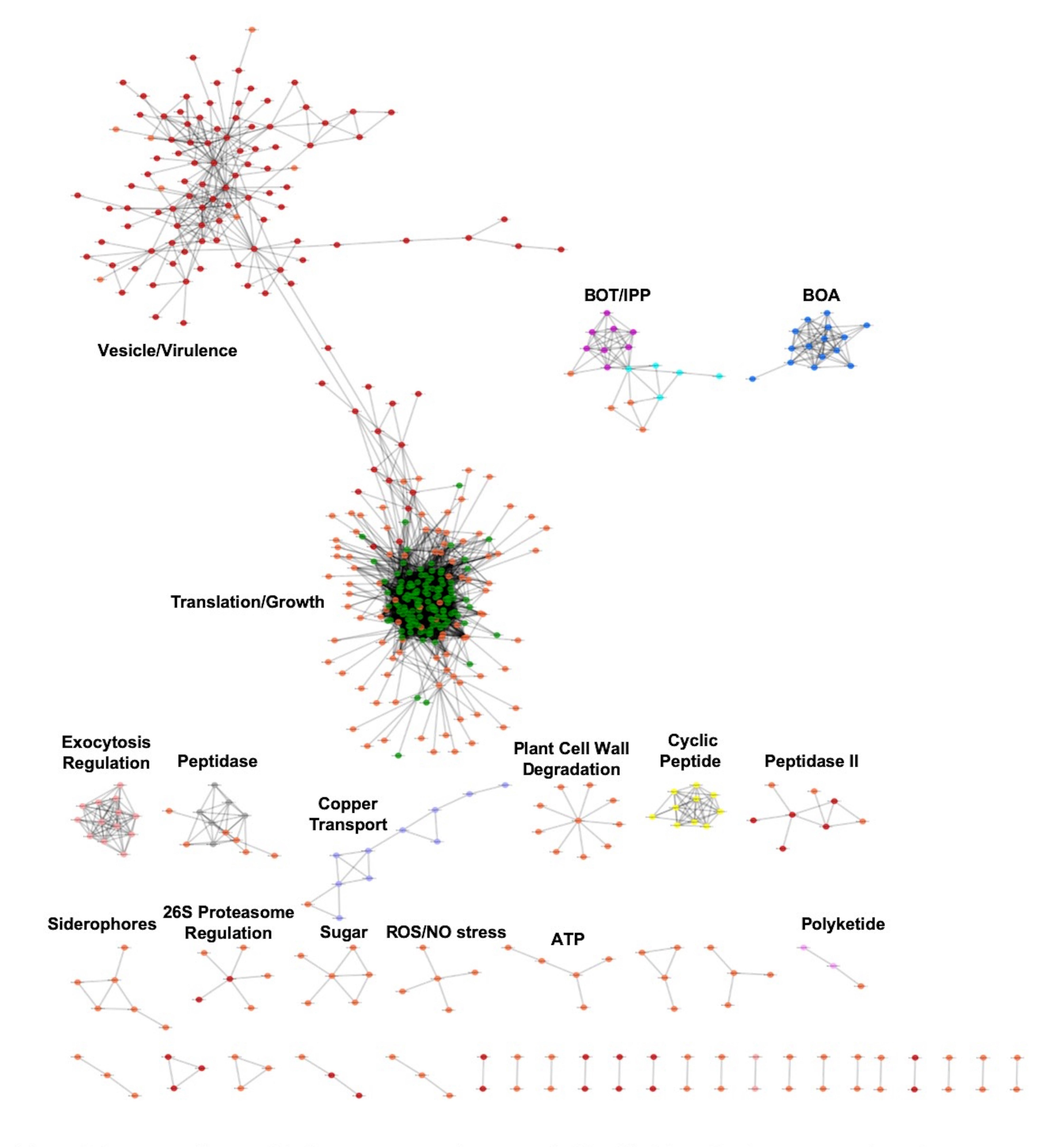


Figure 7-figure supplemental 2. Gene co-expression networks identified from *B. cinerea* transcriptomic responses to Arabidopsis jasmonate-compromised immunity. *B. cinerea* gene co-expression networks (GCNs) were identified from 96 *B. cinerea* isolates infecting on Arabidopsis jasmonate insensitive mutant *coi1-1*. The similarity matrix is computed using Spearman's rank correlation coefficient. All co-expressed gene pairs with correlation greater than 0.8 were shown. Nodes with different colors represent *B. cinerea* genes condensed in GCNs with different biological functions. Nodes were marked with same color as under Arabidopsis wild-type Col-0 background. Nodes specificaly condenced in GCNs under Arabidopsis mutant *coi1-1* background are marked with orange color. Edges represent the Spearman's rank correlation coefficients between gene pairs. GCNs were ordered as number of nodes within each network. GCNs were named after their biological functions, which were determined by hub and bottleneck genes within each network: vesicle/virulence (red/orange), translation/growth (green/orange), botrydial/ isopentenyl pyrophosphate (BOT/IPP, blue/turquoise/orange), botcinic acid (BOA, blue), exocytosis regulation (pink), peptidase (gray/orange), copper transport (slate blue/orange), plant cell wall degradation (orange), cyclic peptide (yellow), peptidase II (red/orange), siderophores (orange), 26S proteasome regulated protein degradation (red/orange), sugar, ROS/NO stress (orange), ATP (orange), polyketide (violet/orange).

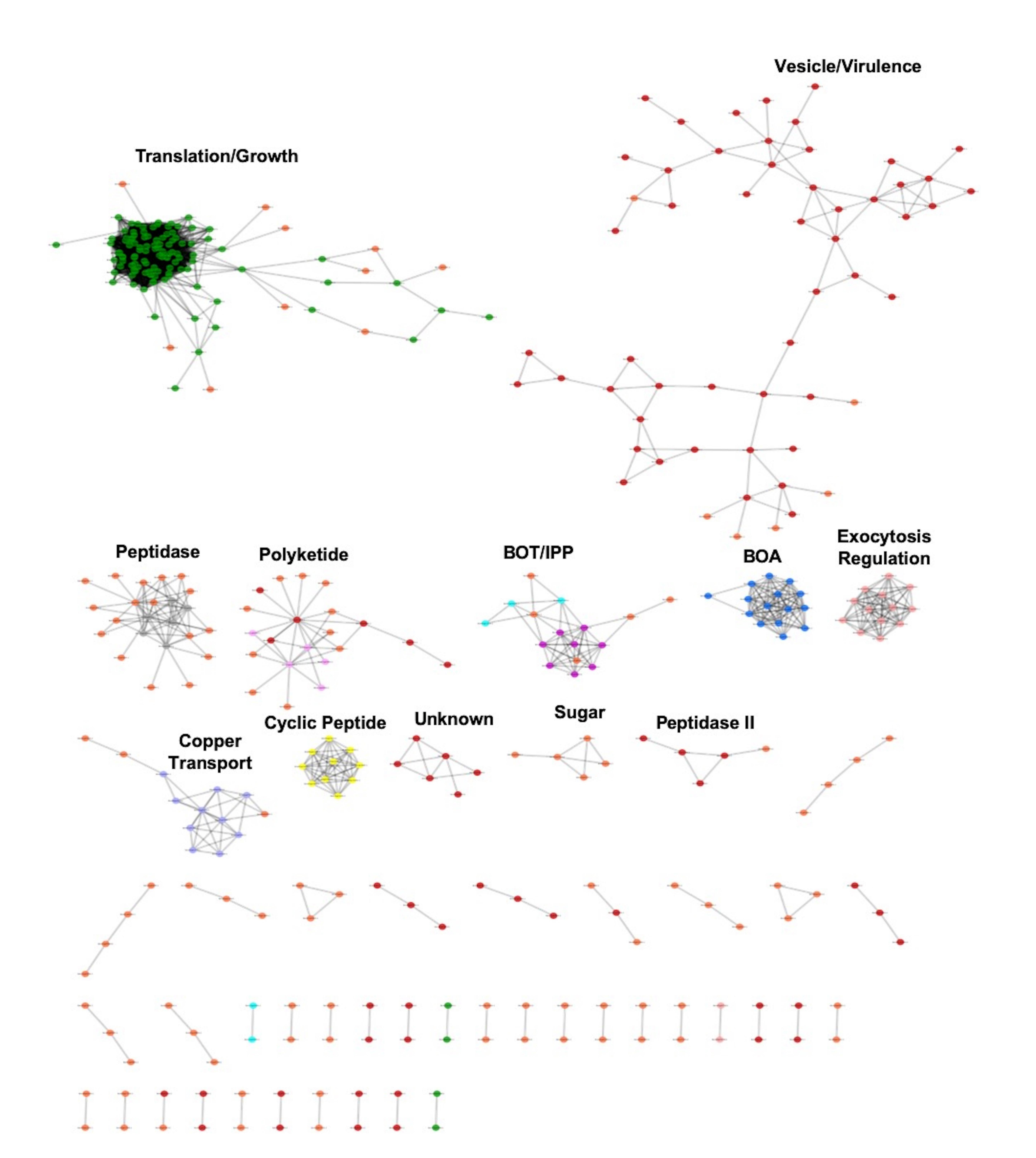
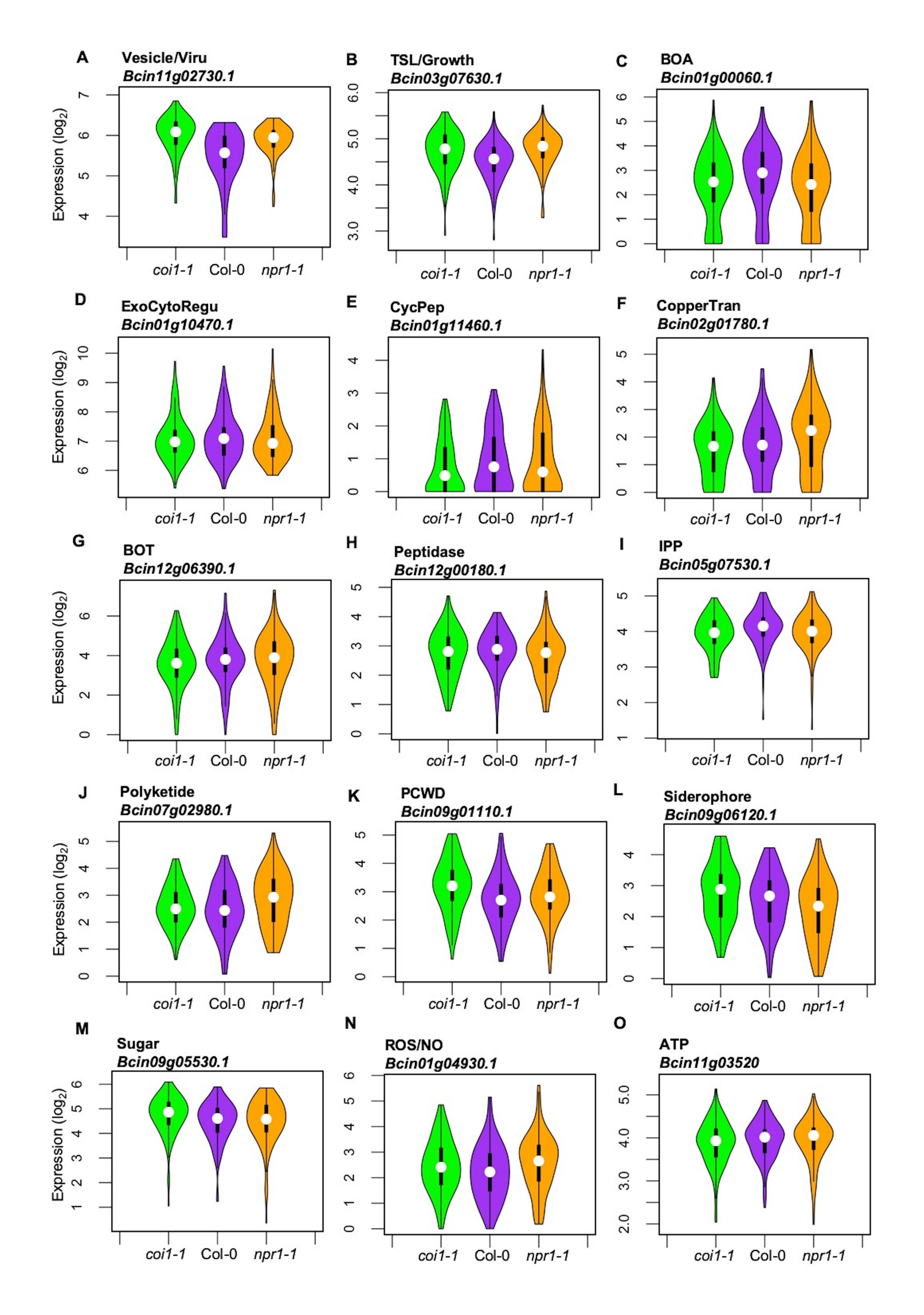


Figure 7-figure supplemental 3. Gene co-expression networks identified from *B. cinerea* **transcriptomic responses to Arabidopsis salicylic acid-compromised immunity.** *B. cinerea* gene co-expression networks (GCNs) were identified from 96 *B. cinerea* isolates infecting on Arabidopsis salicylic acid insensitive mutant *npr1-1*. The similarity matrix is computed using Spearman's rank correlation coefficient. All co-expressed gene pairs with correlation greater than 0.8 were shown. Nodes with different colors represent *B. cinerea* genes condensed in GCNs with different biological functions. Nodes were marked with same color as under Arabidopsis wild-type Col-0 background. Nodes specificaly condenced in GCNs under Arabidopsis mutant *npr1-1* background are marked with orange color. Edges represent the Spearman's rank correlation coefficients between gene pairs. GCNs were ordered as number of nodes within each network. GCNs were named after their biological functions, which were determined by hub and bottleneck genes within each network: translation/growth (green/orange), vesicle/virulence (red/orange), peptidase (gray/orange), polyketide (violet/orange), botrydial/isopentenyl pyrophosphate (BOT/IPP, blue/turquoise/orange), botcinic acid (BOA, blue), exocytosis regulation (pink), copper transport (slate blue/orange), cyclic peptide (yellow), unknown (red), sugar (orange), peptidase II (red/orange).

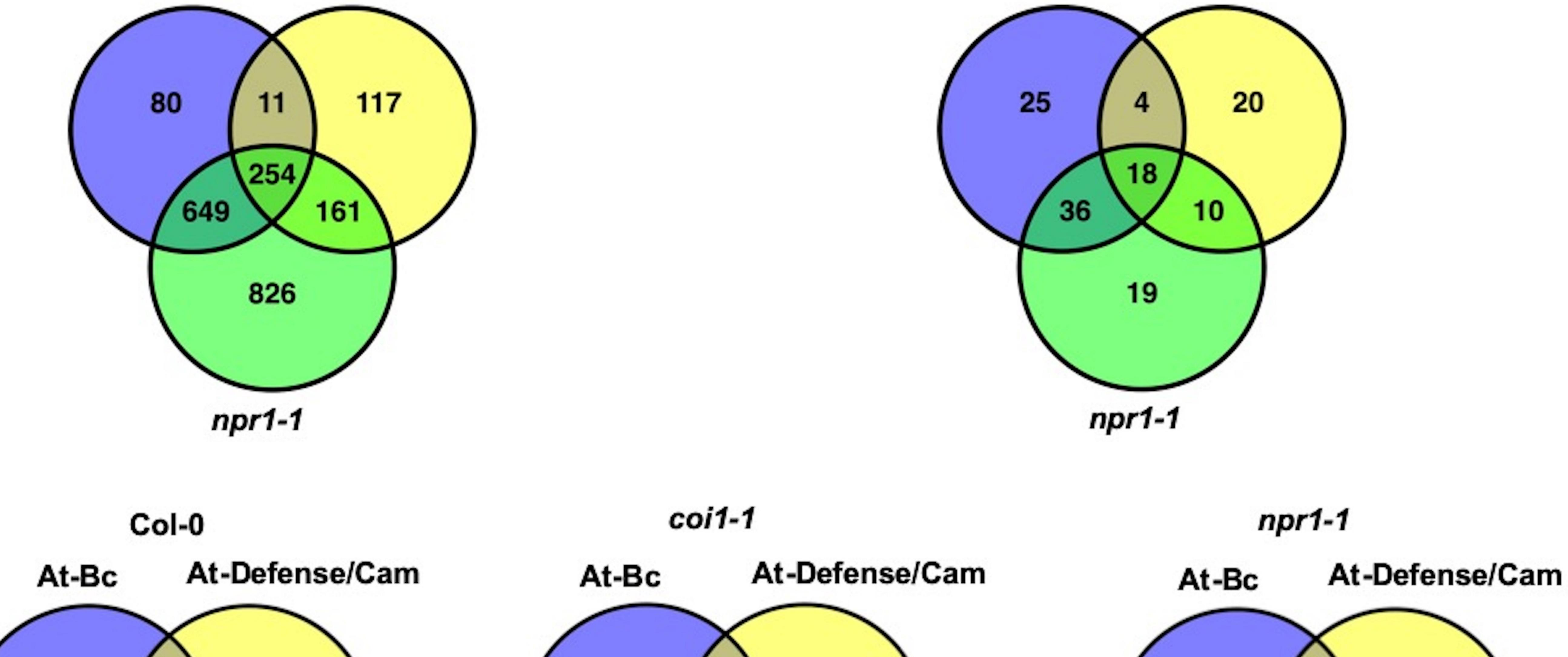


A Plant genes condensed in At-Bc GCNs

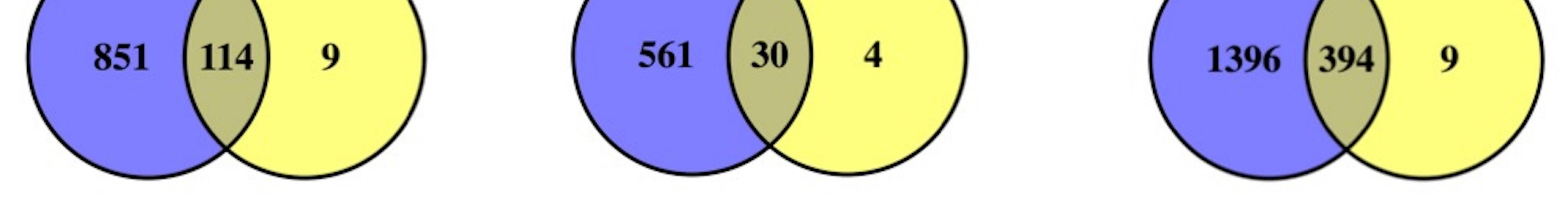
Col-0 coi1-1

Pathogen genes condensed in At-Bc GCNs

Col-0 coi1-1



В



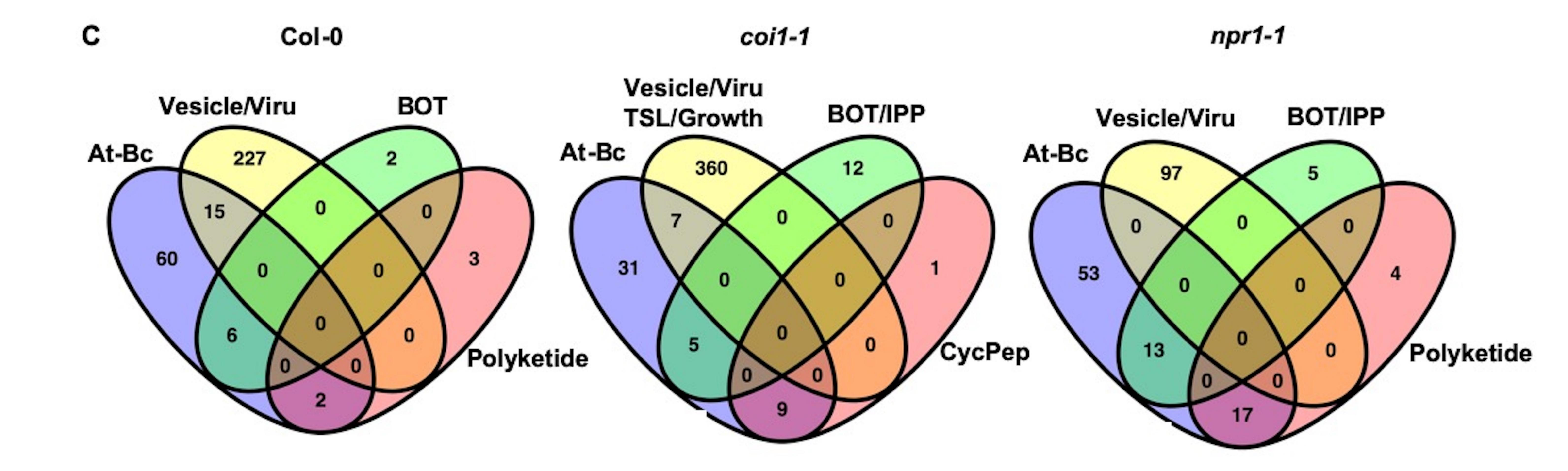
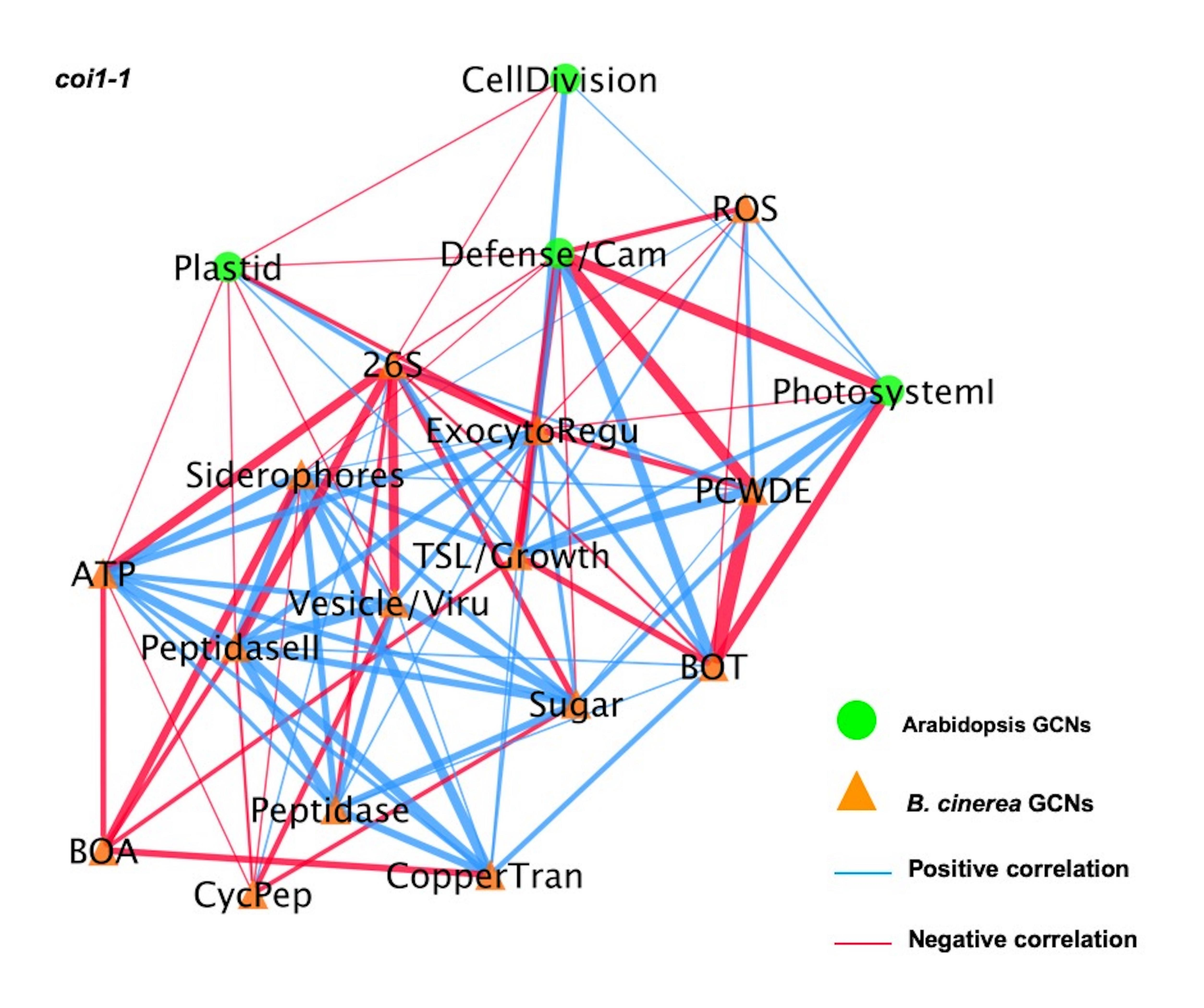


Figure 8-figure supplemental 1. Associations between gene co-expression networks identified from co- and single-transcriptome. Venn diagrams highlights: (A) the overlap of plant (left) and pathogen (right) genes condensed in Arabidopsis-*B. cinerea* gene co-expression networks (GCNs) across three Arabidopsis genotypes, (B) the overlap of plant genes in Arabidopsis-B. cinerea GCNs and Arabidopsis GCNs across three genotypes, (C) the overlap of pathogen genes in Arabidopsis-*B. cinerea* GCNs and *B. cinerea* GCNs across three genotypes.



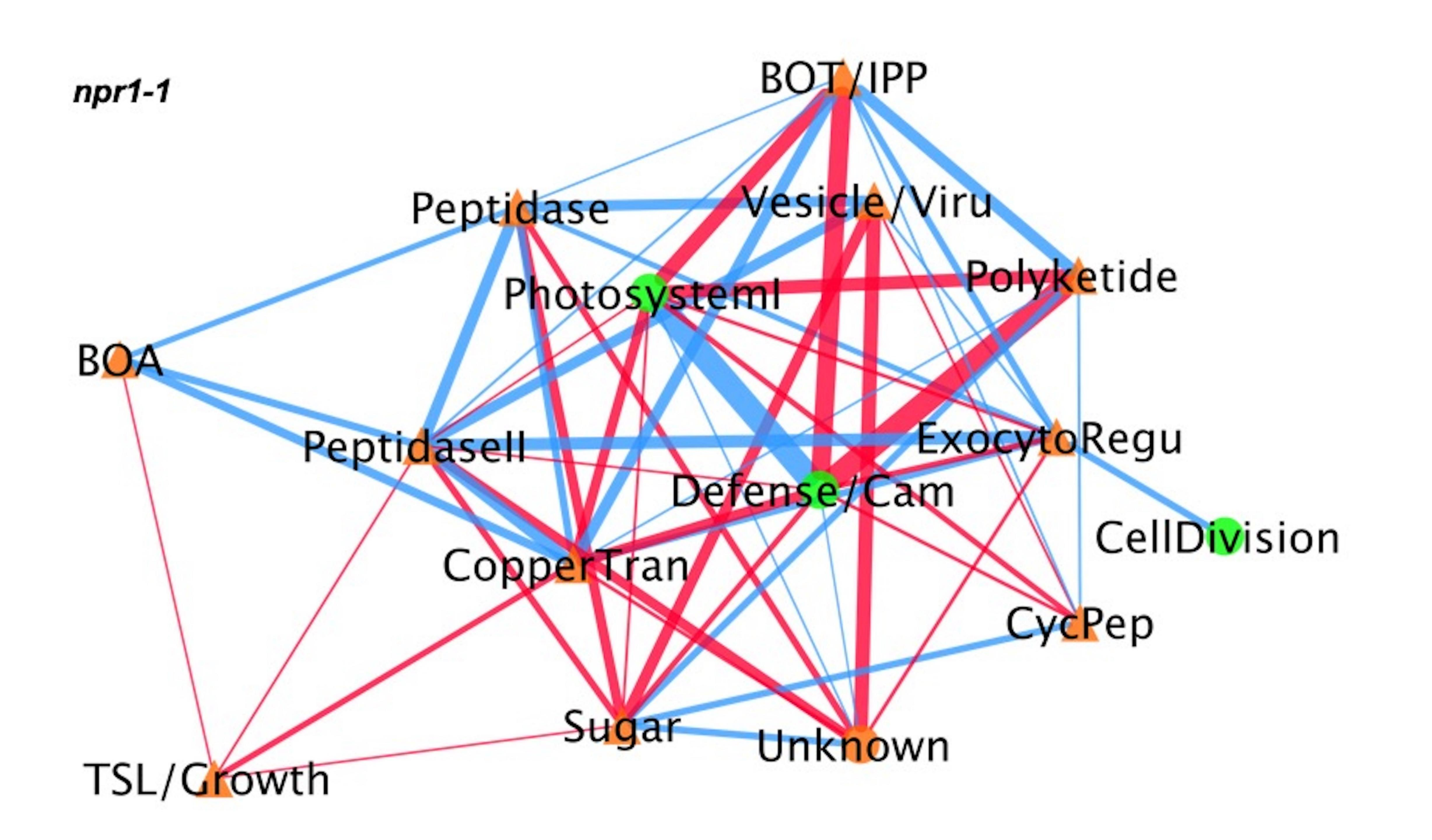


Figure 9-figure supplemental 1. Dual networks reveal links between Arabidopsis immunity and *B. cinerea* **virulence under** *coi1-1* **and** *npr1-1***.** Dual interaction networks were constructed using gene co-expression networks (GCNs) from Arabidopsis and *B. cinerea* co-transcriptome under JA-insensitive mutant *coi1-1* and SA-insensitive mutant *npr1-1*, respectively. The first eigenvectors were derived from individual GCNs and used as input to calculate Spearman's rank correlation coefficiency between GCN pairs. Green dots and orange triangles (nodes) represent Arabidopsis immune- and *B. cinerea* virulence-GCNs, respectively. Blue and red lines (edges) represent the positive and negative Spearman's rank correlation coefficients between GCN pairs, respectively. The thickness of line signifies the correlational strength.

∞ -

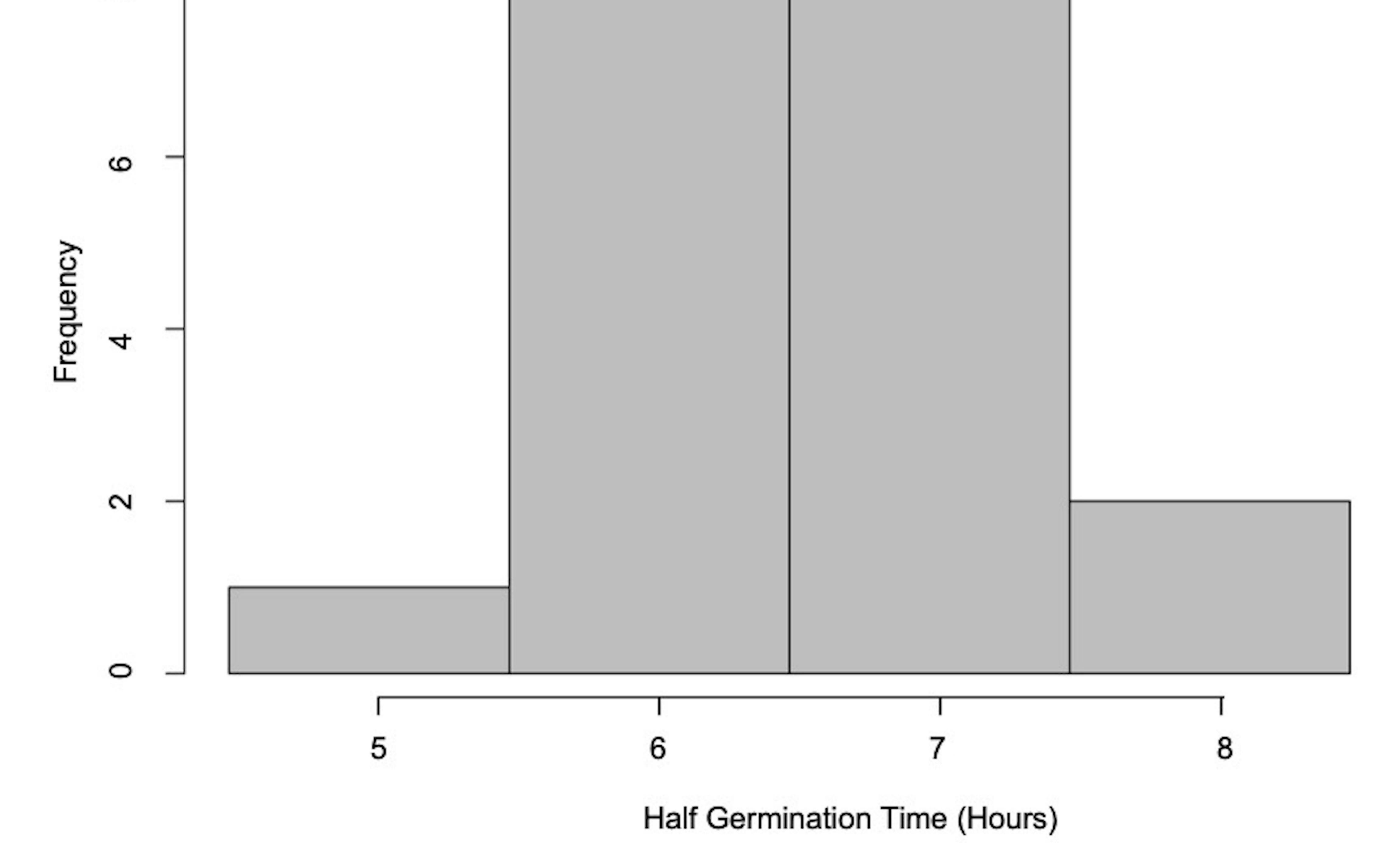


Figure 9-figure supplemental 2. Variation of B. cinerea spore germination time under in vitro condition.